Cellular Signalling 53 (2019) 22–38

Contents lists available at ScienceDirect

Cellular Signalling

journal homepage: www.elsevier.com/locate/cellsig

Elucidating the microRNA-203 specific biological processes in glioblastoma cells from comprehensive RNA-sequencing transcriptome profiling

Bhavesh K. Ahir, Sajani S. Lakka*

Section of Hematology and Oncology, Department of Medicine, University of Illinois College of Medicine at Chicago, Chicago, IL 60612, USA

ARTICLE INFO

Keywords:
Glioblastoma (GBM)
microRNA-203 (miR-203)
High-throughput RNA-sequencing
BCL2 signaling

ABSTRACT

Glioblastoma (GBM) is the most common primary malignant intracranial adult brain tumor. Allelic deletion on chromosome 14q plays an essential role in GBM pathogenesis, and this chromosome 14q site was thought to harbor multiple tumor suppressor genes associated with GBM, a region that also encodes microRNA-203 (miR-203). This study was conducted to identify whole transcriptome profile changes associated with miR-203 expression by high-throughput RNA sequencing. Enrichment analyses for gene ontology (GO) and Kyoto Encyclopedia of Genes and Genomes (KEGG) pathway analysis revealed that miR-203 expression had a strong, negative effect on a number of fundamental and interconnected biological processes involved in cell growth and proliferation. The biological processes mostly influenced were p53 signaling pathway, FoxO signaling pathway, DNA replication, cell cycle, MAPK signaling pathway, and apoptosis. In total, 847 upregulated and 345 downregulated differentially expressed genes were identified in control versus miR-203 expressing glioma cells. After GO enrichment, the downregulated differentially expressed genes such as BCL2, SPARC were found to be mainly enriched in cell cycle regulation and apoptosis processes, whereas the upregulated differentially expressed genes such as CCND1, E2F1 were involved in the DNA replication and cell cycle regulation. We also performed miR-203 target analysis and found BCL2, AKT, SPARC, ROBO1, c-JUN, PDGFA, and CREB were predicted target of miR-203 and miR-203 expression suppressed the protein and mRNA levels of these target genes by western blotting and qRT-PCR analysis. Moreover, co-transfection experiments using a luciferase-based reporter assay demonstrated that miR-203 directly regulated BCL-2 expression and BCL-2 overexpression suppressed miR-203 mediated glioma cell apoptosis. These results indicate that overexpression of miR-203 coordinately regulates several oncogenic pathways in GBM.

1. Introduction

Glioblastoma (GBM) is the most frequently occurring primary malignant intracranial tumor arising from glial cells in the adult brain, and account for 60–80% of all brain tumors [1,2]. Based on the WHO recent classification of central nervous system tumors, diffuse gliomas are categorized into four grades (I-IV) according to World Health Organization (WHO): diffuse astrocytoma (IDH mutant, WHO grade-II), oligodendroglioma (IDH mutant, WHO grade-II), anaplastic oligodendroglioma (IDH mutant, WHO grade-II), anaplastic astrocytoma (IDH mutant, WHO grade-III), and glioblastoma (IDH mutant, WHO grade-IV) [3–5]. Moreover, among all glioma cases diagnosed, astrocytoma grade III or GBM is considered to be the most severe and incurable form of glioma due to poor prognosis and high invasiveness [6]. Despite aggressive treatments, the median survival for patients diagnosed with GBM has only marginally improved over the last decades and remains about 2% with a median survival rate of 1 year [7,8]. Moreover, the molecular mechanisms underlying GBM progression remain poorly elusive [9]. Hence, the development of novel approaches to identify molecular determinants of GBM progression holds promise for the development of new therapeutic approaches.

microRNA (miRNA) are small non-coding RNA endogenous molecules consisting of 19–25 nucleotides in length that regulate expression of specific genes through binding to the 3′ untranslated region (3'UTR) of target mRNAs, which eventually results in either mRNA degradation or translation repression [10]. It is well established that a single miRNA can regulate multiple target genes simultaneously, while a single gene may be regulated by multiple miRNAs [11]. In recent years, emerging evidence suggests that miRNAs have comprehensive biological functions and are involved in a wide range of fundamental biological processes including cell survival, cell proliferation, cellular differentiation, apoptosis and migration [12–14]. Furthermore, over half of the miRNAs

* Corresponding author.
E-mail address: slakka@uic.edu (S.S. Lakka).

https://doi.org/10.1016/j.cellsig.2018.09.014
Received 9 August 2018; Received in revised form 19 September 2018; Accepted 19 September 2018
Available online 20 September 2018
0898-6568/

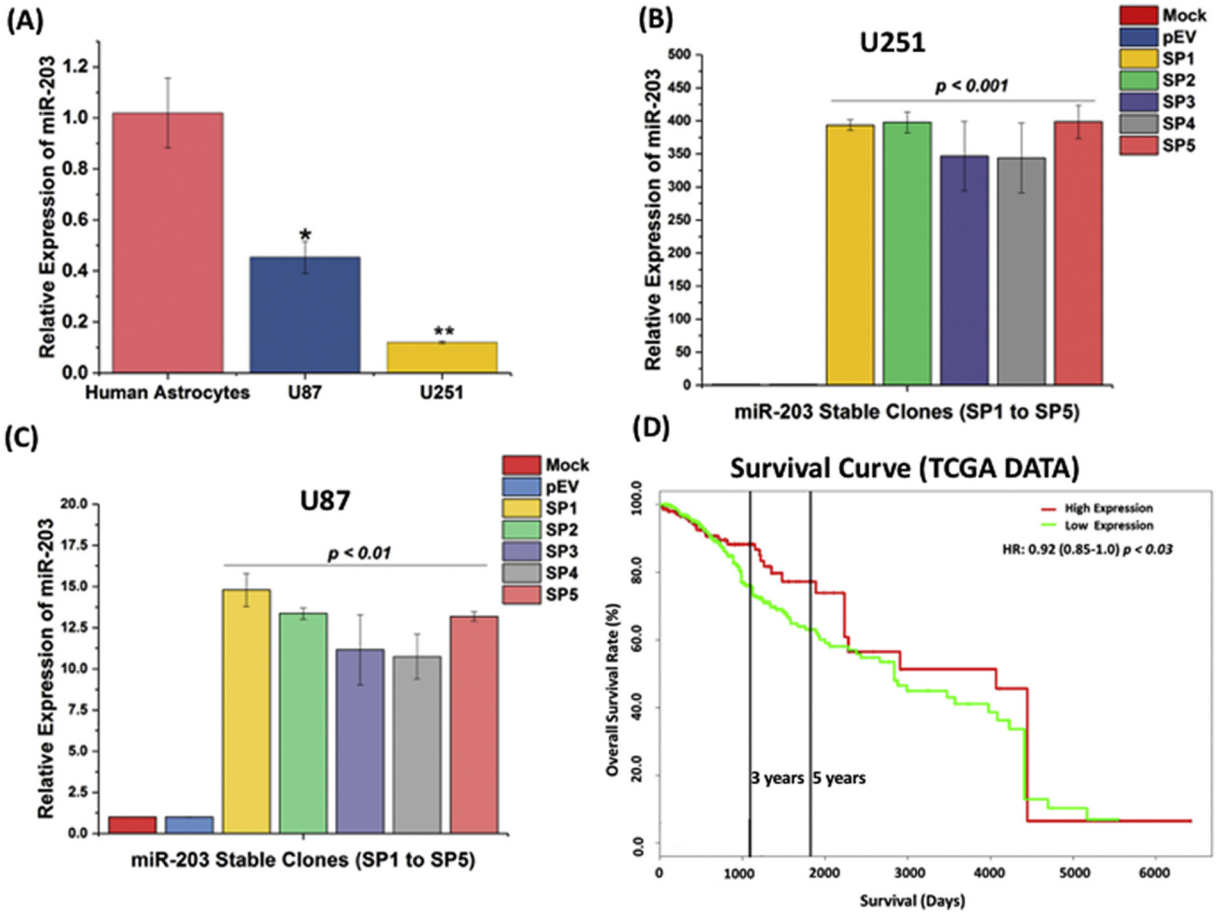

Fig. 1. miR-203 expression in glioma cells and GBM cancer patient samples. Total RNA was extracted using TRIzol reagents, and qRT-PCR was performed for assessment of miR-203 expression level with U6 snRNA as a normalization control (Mean ± S.E., n = 3). *$p < .05$ vs. normal control samples; **$p < .01$ vs. normal control samples. (A) qRT-PCR was performed to determine the expression level of miR-203 in human astrocytes and glioma cell lines (U251 and U87). Glioma cells (U251 and U87) were transfected with the pTarget plasmid containing has-miR-203 precursor (pmiR-203) and empty vector control (pEV) or Mock for 36 h. The stable cell lines overexpressing miR-203 were designated as U251-SP or U87-SP. (B) miR-203 expression by qRT-PCR in U251 cells and (C) miR-203 expression by qRT-PCR in U87 Cells. (D) miR-203 expression in the TCGA database of 648 lower grade glioma (LGG) patient samples with accompanying survival information was related to overall patient survival ($p = .03$). High miR-203 LGG patients had significantly longer survival (2–3 fold) as compared to patients with low miR-203 expression.

are located in cancer-related genomic signatures and the deregulation of certain miRNAs have been found to be closely associated with certain types of cancer including GBM where they play a dual role as oncogenes or tumor suppressors [12,15,16].

The aberrant expression of miR-203 has been found to be significantly downregulated in various types of cancer, including melanoma, prostate cancer, colon cancer, hepatocellular carcinoma, esophageal squamous lung carcinoma, laryngeal cancer and GBM [17–22]. It has been shown that miR-203 is known for its tumor suppressive activity by negatively regulating cell proliferation, cell invasion and chemotherapeutic intervention [23,24]. In addition, recent studies have shown that downregulation of miR-203 is associated with chemoresistance in human GBM by promoting epithelial-mesenchymal transition (EMT) via SNAI2 [25]. In our previous studies, we have shown that overexpression of miR-203 significantly suppresses ROBO1 which in turns suppress ERK phosphorylation and MMP-9 expression thereby repressing glioma cell invasion and migration by disrupting the ROBO1/ERK/MMP-9 signaling cascade [23]. However, the function of miR-203 in other biological processes remains to be fully elucidated in GBM as well as miR-203 target several components of various pathways that result into the alteration of various molecular networks in tumor progression. Our goal was to profile novel and differentially expressed genes that were altered by miR-203 expression. We compare the gene expression profiles in the presence and absence of miR-203 using the comprehensive RNA-seq transcriptome profiling. Using bioinformatics and systems biology approach, we systematically identified differentially expressed genes, novel genes, and transcripts, biological pathways, alternative splice variants in miR-203 expressing cells. We also validate our RNA-seq differentially expressed genes which were found to be enriched in the apoptosis process via miR-203 modulation in glioma cells via qRT-PCR. Furthermore, we also performed the separate miR-203 target analysis and demonstrated that the total protein and gene expression levels of miR-203 predicted targets such as SPARC, BCL2, AKT, ROBO1, c-JUN, CREB, and PDGFA were significantly downregulated in miR-203 expressing glioma cell compared to controls. Our study also revealed enforced BCL2 expression mediates miR-203 induced apoptosis in glioma cells. Taken together, the results of our study shows that miR-203 expression regulates cellular pathways this is likely to impact therapy resistance in GBM.

2. Materials and methods

2.1. Cells and culture condition

We used the U251and U87 glioma cell lines for this study. Human astrocytes cell line, U251 and U87 cell lines were obtained from American Type Culture Collection (ATCC, Rockville, MD). To obtain consistent results, cells were frozen at third or fourth passage. U251 and

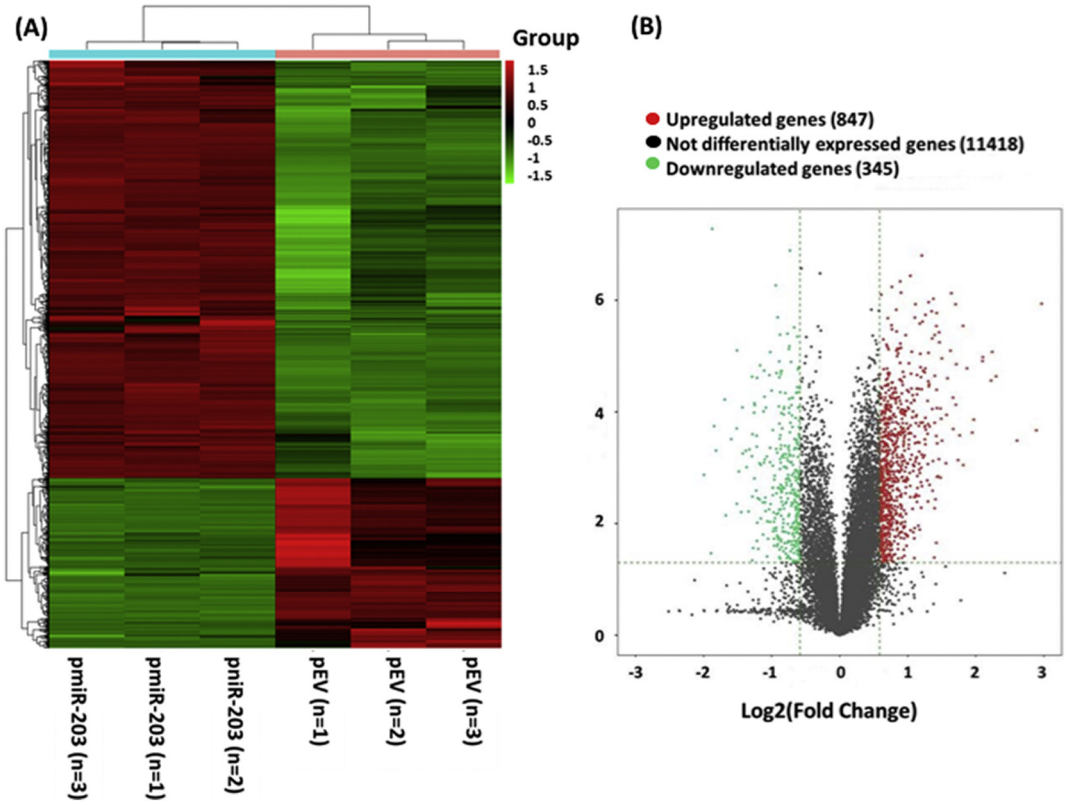

Fig. 2. Heatmap for hierarchical clustering of differentially expressed genes (DEGs) across pEV versus pmiR-203 stable U25 cells. (A) shows the unsupervised hierarchical clustering of the 1192 DEGs. Heatmap color scale represents upregulated genes (Red) or downregulated genes (Green). (B) indicates Volcano Plot of DEGs. Red/Green circles indicate statistically significant DEGs with fold change no < 1.5 and $p \leq .05$ between the pEV versus pmiR-203 samples. (For interpretation of the references to color in this figure legend, the reader is referred to the web version of this article.)

U87 cells were cultured in DMEM (Gibco-BRL, Grand Island, NY) media supplemented with 10% FBS (Sigma-Aldrich, MO, USA), 2 mMl^{-1}L-glutamine (Invitrogen, Carlsbad, CA), 100 Uml^{-1} penicillin and 100 μgml^{-1} streptomycin (Gibco-BRL, Grand Island, NY), and cells were maintained in a humidified atmosphere containing 5% CO_2 at 37 °C.

2.2. miR-203 plasmid construction, cell transfection and miR-203 stable cell lines generation

We constructed the human precursor miR-203 (hsa-miR-203) as described previously [23] and the sequence was amplified by PCR using following human precursor miR-203 forward (F) and reverse (R) primers: miR-203-F, 5'-AGCTCGGCGAACCGACGGTGTT-3′, miR-203-R, 5'-CCTGACTGTGACTCTGACTCCA-3′ (IDT, San Jose, CA), then cloned into phCMV-C-Luc plasmid (Genlantis, San Diego, CA) after the stop codon using pTarget TA cloning vector (Promega, Madison, WI). White colonies were selected for screening with the restriction enzyme that releases the insert, and the orientation was determined by sequencing.

U251 and U87 cells were transfected with a pTarget plasmid containing hsa-miR-203 precursor and pEV (a pcDNA vector carrying no insert) using FuGene®HD (Roche, Indianapolis, IN) as per manufacturer's instructions. For the transfections, cells were cultured either in 100 mm dishes until 60% to 80% confluence were obtained. 1 and 2 µg of plasmid DNA were mixed with FuGene®HD in serum-free medium per manufacturer's instructions, and 30 min later added to the cells. After allowing 8-h (h) for optimal transfection, the serum-free medium was replaced by complete, supplemented medium, and cells were incubated for 36 h. Cells were harvested for the collection of whole cell lysate for western blotting analysis and quantitative reverse polymerase chain reaction (qRT-PCR) analysis.

We developed stable cell lines stably expressing miR-203 and pEV using U251 and U87 GBM cells lines and cells were selected with cloning cylinders after 3–4 weeks in medium containing G418. Wild-type U251 and U87 cells are termed as U251 and U87 parental (U251-Mock and U87-Mock) and the stable cell lines overexpressing miR-203 were designated as U251-SP and U87-SP, whereas U251-EV and U87-EV were the cell lines were transfected stably with the empty vector.

3. miR-203 expression analysis in glioma cells using quantitative reverse transcription PCR (qRT-PCR)

To check the expression of miR-203 levels in glioma and human astrocytes cells, we have next performed the miRNA specific qRT-PCR analysis. Total RNA was extracted from these cells using a miRNeasy Mini Plus kit (Qiagen, Valencia, CA) with QIAzol Lysis Reagent (Qiagen, Valencia, CA) for cell lysis. The RNA isolation procedure was accomplished using manufacture's instruction. 1 µg of total RNA was used as a template for reverse transcription reaction using the miScript II Reverse Transcription kit (Qiagen, Valencia, CA), accordingly to the manufacturer's instructions using 5× miScript HiFlex Buffer, which enables conversion of mature as well as precursor miRNAs. qRT-PCR was performed in 25 µl reaction using the miScript SYBR Green PCR kit (Qiagen, Valencia, CA), has-miR-203 forward primer 5'-GCG TGA AAT GTT TAG GAC CAC TAG- 3′, and the reference U6 housekeeping miRNA in combination with the miScript Universal reverse primer (supplied with miScript SYBR Green PCR kit) for the cDNA templates. qRT-PCR reactions were performed in triplicate and independently repeated at least twice with no template control on 7500HT Fast Real-Time PCR System (Applied Biosystems, Carlsbad, CA, USA). PCRs were processed through an initial denaturation at 95 °C for 15 min and by 40 cycles of 3-step PCR, including 15 s of denaturation at 94 °C, a 30 s annealing phase at 55 °C and an elongation phase at 70 °C for 34 s. The resulting

Table 1
Top 25 upregulated differentially expressed genes in miR-203 stable U251 cells compared to U251 pEV control cells.

Gene Symbol	Locus	Fold Change	p-value	Description
KRT81	Chr12-	7.82621611	1.15E-06	Keratin 81
LY6E	Chr8+	7.420388681	2.14E-04	Lymphocyte Antigen 6 Family Member E
FAM20C	Chr7+	6.086635318	3.27E-04	Family with Sequence Similarity, Member C
XAGE1E	ChrX-	4.922232721	2.30E-05	X Antigen Family Member 1E
SCUBE3	Chr6+	4.730741228	8.42E-06	Signal Peptide, CUB Domain and EGF Like Domain Containing 3
PCSK1N	ChrX-	4.676156471	2.75E-05	Proprotein Convertase Subtilisin/Kexin Type I Inhibitor
XAGE1A	ChrX-	4.302797545	1.05E-05	X Antigen Family Member 1A
XAGE1D	ChrX-	4.285838454	1.23E-05	X Antigen Family Member 1D
HAS2	Chr8-	3.921240463	1.37E-04	Hyaluronan Synthase 2
CXCL14	Chr5-	3.860667121	2.35E-04	C-X-C Motif Chemokine Ligand
TSEN15	Chr1+	3.658675369	1.66E-05	TRNA Splicing Endonuclease Subunit 15
SIRPA	Chr20+	3.520715978	8.96E-04	Signal Regulatory Protein Alpha
SOSTDC1	Chr7-	3.515099325	2.88E-06	Sclerostin Domain Containing 1
MAGEH1	ChrX+	3.394941649	2.63E-04	MAGE Family Member H1
SALL3	Chr18+	3.341938922	7.28E-04	Spalt Like Transcription Factor 3
FAM111B	Chr11+	3.282073244	1.40E-05	Family with Sequence Similarity 111, Member B
TXNIP	Chr1+	3.267512234	7.43E-05	Thioredoxin Interacting Protein
MAGEA11	ChrX+	3.258541083	1.18E-06	MAGE Family Member A11
MYBL2	Chr20+	3.178863818	2.02E-04	MYB Proto-Oncogene Like 2
FRMD3	Chr9-	3.17459609	5.54E-05	FERM Domain Containing 3
XAGE1C	ChrX+	3.12112058	7.49E-07	X Antigen Family Member 1C
ID3	Chr1-	3.091924962	8.01E-06	Inhibitor of DNA Binding 3, HLH Protein
BASP1	Chr5+	3.001418814	2.50E-05	Brain Abundant Attached Signal Protein
TMEM59L	Chr19+	2.972467724	1.13E-04	Transmembrane Protein 59 Like

Table 2
Top 25 downregulated differentially expressed genes in miR-203 stable U251 cells compared to U251 pEV control cells.

Gene Symbol	Locus	Fold Change	p-value	Description
PAGE5	ChrX+	0.250547752	1.34E-03	PAGE Family Member 5
AC007192.4	Chr19+	0.269352863	3.41E-02	Cloned Based Ensemble Gene
C22orf29	Chr22-	0.272456549	5.28E-08	Chromosome 22 Open Reading Frame 29
EDN2	Chr1-	0.278014354	1.79E-04	Endothelin 2
ZNF791	Chr19+	0.283421347	4.93E-04	Zinc Finger Protein 791
KLF2	Chr19+	0.309805177	6.01E-05	Kruppel Like Factor 2
BCL2L11	Chr2+	0.313250552	7.14E-03	BCL2 Like Protein 11
DIRAS3	Chr1-	0.331155184	3.08E-04	DIRAS Family GTPase 3
VCY1B	ChrY+	0.35018256	1.98E-04	Variable Charge, Y-linked 1B
PPL	Chr16-	0.350285024	4.43E-03	Periplakin
SFRP4	Chr7-	0.351060832	7.94E-06	Secreted Frizzled Related Protein 4
VCY	ChrY-	0.357910132	1.17E-03	Variable Charge, Y-linked
TIMP3	Chr22+	0.366556589	6.23E-03	TIMP Metallopeptidase Inhibitor 3
SERPINE1	Chr7+	0.371028263	8.31E-05	Serpin Family E Member 1
ALDH3A1	Chr17-	0.372266924	5.56E-04	Aldehyde Dehydrogenase 3 Family Member A1
JUNB	Chr19+	0.384275007	4.97E-04	June B Proto-Oncogene
CNTN1	Chr12+	0.387350227	9.78E-04	Contactin 1
MSLN	Chr16+	0.394958818	6.08E-03	Mesothelin
PER1	Chr17-	0.398562408	4.71E-04	Period Circadian Regulator 1
FSTL3	Chr19+	0.40884638	6.21E-04	Follistatin Like 3
PIK3AP1	Chr10-	0.409380424	2.34E-05	Phosphoinositide-3-Kinase Adaptor Protein 1
HILPDA	Chr7+	0.409688887	4.56E-02	Hypoxia Inducible Lipid Droplet Associated
BBC3	Chr19-	0.410784516	3.30E-03	BCL2 Binding Component 3
IRS2	Chr13-	0.41097674	2.51E-04	Insulin Receptor Substrate 2
DEDD2	Chr19-	0.414169405	2.75E-02	Death Effector Domain Containing 2

RT-PCR cycle times were normalized against the U6 housekeeping miRNA, and fold change (FC) values of miRNA expression was calculated using the ΔΔCt method. Fold changes compared to controls were calculated by $2^{-\Delta\Delta Ct}$ after normalizing to U6, a reference gene. Statistical significance of the difference in miR-203 expression levels between these cells or pmiR-203 expression levels between the empty vehicle (pEV) control or mock control samples were calculated by unpaired *t*-tests in GraphPad Prism 5 Software (GraphPad Software Inc., San Diego, CA).

3.1. TCGA database analysis

To examine the relationship between miR-203 and glioma patients, we also mined the Human Cancer Genome Atlas (TCGA) database and TCGA data portal for all samples with level 3 miRNA data or mRNA expression data available as well as the accompanying clinical data. The dataset was filtered for samples having expression data for has-miR-203 for high ($n = 160$) and low expression GBM patients ($n = 480$), yielding a final set of 648 GBM. The student *t*-test was used for analyzing the differences between indecent datasets were performed using Grapad Prism 5 Software (GraphPad Software Inc., San Diego, CA). Overall survival of GBM patients with high and low levels of miR-203 based on TCGA dataset were shown by using a Kaplan-Meier curves to present the prognosis of the high and low groups. The Wilcoxon log rank test was then used on the Kaplan-Meier curves to detect the survival difference between these two groups.

3.2. High-throughput RNA-sequencing

For whole transcriptome analysis, total RNA was extracted from miR-203 expressing U251 stable cell lines (pmiR-203) and pEV control samples in biological triplicate. RNA extractions were performed using RNeasy Mini Kit (Qiagen Inc., Valencia, CA) with DNase treatment on column following manufacture's instruction. Quality control of the total RNA samples were quantified using a NanoDrop ND-1000 instrument and qualified using agarose gel electrophoresis. Briefly, RNA-sequencing (RNA-seq) was performed by the Illumina HiSeq 4000 system using the standard pair-end sequencing protocol. Approximately 70 to 80 million 150-bp paired reads were obtained and mapped to the reference genome. 1 to 2 μg total RNA was used to prepare the sequencing library in the following steps: (1) Total RNA was enriched by oligo (dT) magnetic beads (rRNA removed) and (2) RNA-seq library was prepared using KAPA Stranded RNA-Seq Library Prep Kit (Illumina), which incorporates dUTP into the second cDNA strand and renders the RNA-seq library strand-specific. (3) The completed libraries were qualified with Agilent 2100 Bioanalyzer and quantified by absolute quantification qRT-PCR method. To sequence the libraries on the Illumina HiSeq 4000 instrument, the barcoded libraries were mixed, denatured to single-stranded DNA in NaOH, captured on Illumina flow cell, amplified in situ, and subsequently sequenced for 150 cycles for both ends on Illumina HiSeq instrument.

3.3. RNA-seq analysis

Image analysis and base calling were performed using Solexa

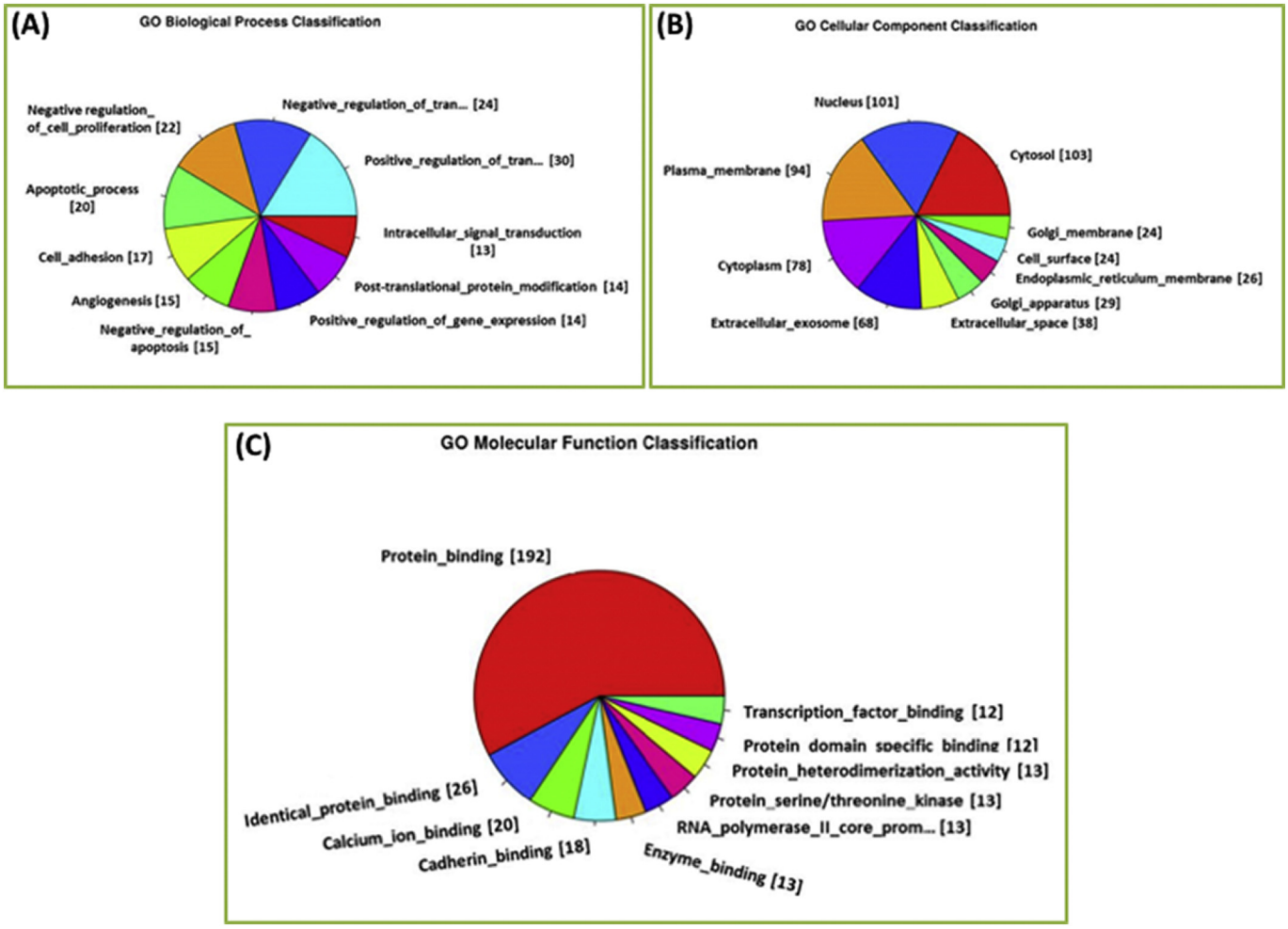

Fig. 3. Gene Ontology (GO) enrichment analysis of upregulated DEGs in pmiR-203 stable U251 samples versus pEV control samples. (A) Pie charts represent the top 10 significantly altered classification of GO Biological Processes, (B) Cellular Component Classification or (C) Molecular Function as determined by DAVID web tool. The *p-values* ($p \leq .05$) calculated by Fisher's exact test is used to estimate the statistical significance of the enrichment of the pathways between the pEV control versus pmiR-203 treated U251 cells.

pipeline v.18 (Off-Line Base Caller Software, v1.8). The schematic overview of the RNA-seq analysis pipeline is presented in Supplementary Material, Fig. 1. Sequence quality was examined using the FASTQ files using FastQC software. The trimmed sequence reads (trimmed 5′, 3′-adaptor based cutadapt) were aligned to the human reference genome UCSC build hg19 (GRCh37) assembly using Hisat2 software [26,27]. The transcript abundances for each sample was estimated with StringTie [28,29], and gene and transcript level were calculated as FPKM (fragments per kilobase per million mapped reads) using R package Ballgown [28,30–32]. Differentially expressed genes and transcripts from miR-203 stable U251 cells versus control samples were also calculated with R package Ballgown. The novel genes and transcripts were predicted from assembled results by comparing to the reference annotation using StringTie and Ballgown, then use CPAT [33] to assess the coding potential of those sequences. It was required for the differentially expressed genes and transcripts to satisfy both *p-value* and fold change cutoff criteria simultaneously fold change cutoff 1.5, $p \leq .05$ and FPKM ($\geq$ 0.5 means in one group) were used for filtering differentially expressed genes and transcripts. The *p-values* were obtained using the Fisher's exact test and the false discovery rate (FDR) was controlled by the Benjaminin and Hochberg algorithm. The data discussed in this publication have been deposited in NCBI's Gene Expression Omnibus [34] and are accessible through GEO Series accession number GSE119711 (https://www.ncbi.nlm.nih.gov/geo/query/acc.cgi?&acc=GSE119711).

3.4. Functional enrichment analysis

Functional analysis of differentially expressed genes was carried out by the Gene Ontology (GO) project (http://www.geneontology.org) on the basis of three structured relationships of defined terms that describe gene product attributes: biological process (BP), molecular function (MF), and the cellular component (CC). We used GO functional enrichment analysis to investigate whether specific GO terms were more likely to be associated with the differentially expressed genes. The Fisher's exact test was used to classify the GO category, and FDR was calculated to correct the *p-value*. $p \leq .05$ and *q-values* ≤ 1 (FDR adjusted *p-values)* were used as a threshold to select significantly differentiated expressed gene list to categorized GO in terms of BP, MF, and the CC.

3.5. Biological pathway analysis

Based on the latest KEGG database (Kyoto Encyclopedia of Genes and Genomes), we analyzed pathway analysis, the interaction network of the significant pathways of differentially expressed genes from miR-203 U251 stable cells versus U251-EV control samples. Furthermore, the interaction network of the significant pathways of differentially expressed genes was built according to the interaction among pathways of the KEGG database to find out the relationship among the significant pathways directly and systematically. KEGG database is a curated

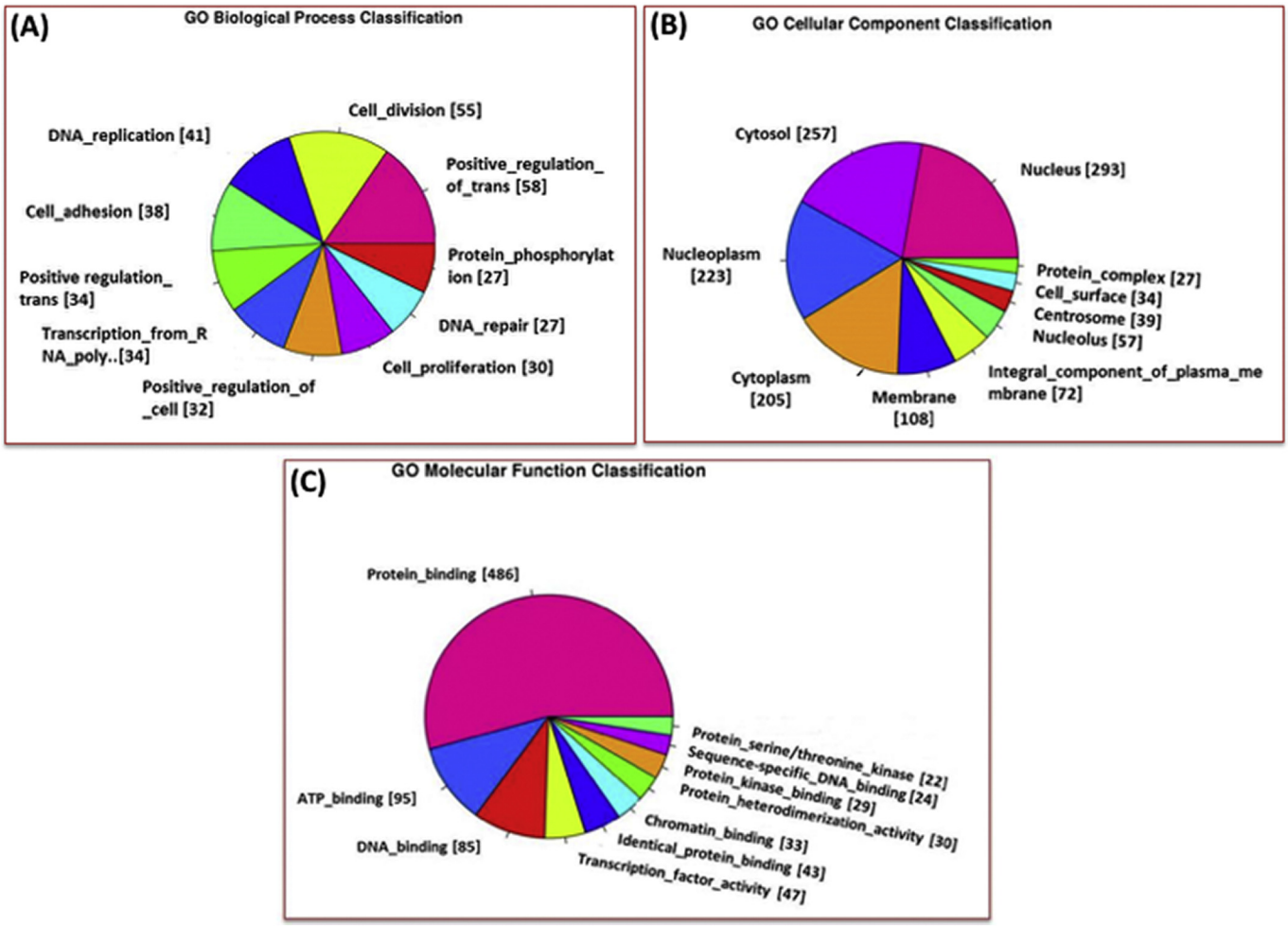

Fig. 4. Gene Ontology (GO) enrichment analysis of downregulated DEGs in pmiR-203 stable U251 samples versus pEV control samples. (A) Pie charts represent the top 10 significantly altered classification of GO Biological Processes, (B) Cellular Component Classification or (C) Molecular Function as determined by DAVID web tool. The *p-values* ($p \leq .05$) calculated by Fisher's exact test is used to estimate the statistical significance of the enrichment of the pathways between the pEV control versus pmiR-203 treated U251 cells.

database of molecular pathways and disease signatures and KEGG acts as a bioinformatics resource for understanding higher order functional meanings and utilizes of the cell or organism from its genome information (http://www.genome.ad.jp/kegg). KEGG pathway analysis demonstrates whether the differentially expressed mRNAs are enriched in certain biological pathways according to their biological functions and disease signature. The Fisher's exact test was used to the statistically significant difference ($p < .05$) of the enrichment of the biological pathways between miR-203 stable U251 cells compared to control cells.

3.6. Gene set enrichment analysis (GSEA)

Gene set enrichment analysis (GSEA) is a computational method that determines whether an a priori defined set of genes shows the statistically significant concordant difference between two biological states such as phenotypes. We used GSEA to identify a set of genes involved in specific pathways and biological pathways, disease signatures involved in miR-203 stable U251 cells compared to control cells.

3.7. Alternative splicing analysis

The differential splicing analysis was based on the Hisat2 alignments to the human reference transcriptome release GRCh37.75 (hg19) in ENSEMBL by dSpliceType [35]. The analysis of alternative splicing changes (the five most common types of splicing events include skipped exon (SE), retained intron (RI), alternative 3′ or 5′ splice sites (A3SS or A5SS), and mutually exclusive exons (MXE)) in the RNA-seq data of miR-203 expressing U251 stable cells versus control samples were performed using dSpliceType. The method utilized sequential dependency of base-wise reads coverage signals and it also includes biological variability among replicates using a multivariate statistical model. dSpliceType substantially reduces sequencing bias by taking ratios of normalized RNA-seq splicing indexes at each nucleotide between disease and control conditions. dSpliceType employs a change-point analysis followed by a parametric statistical test using the Schwarz Information Criterion (SIC) on each candidate splicing event for differentially splicing event detection. It can detect various types of differential splicing events from a wide range of expressed genes including genes with lower abundances. dSpliceType detects differential expression using a multivariate or univariate statistical test based on the global RNA-seq splicing indexes calculated on the left and right common exons (Supplementary Material, Fig. 2).

3.8. Western blot analysis

Glioma U251 and U87 cells were transfected with mock, pEV or pmiR-203 (1 μg/ml and 2 μg/ml) for 36 h as described above, and whole cells lysates were prepared by lysing cells in RIPA lysis buffer

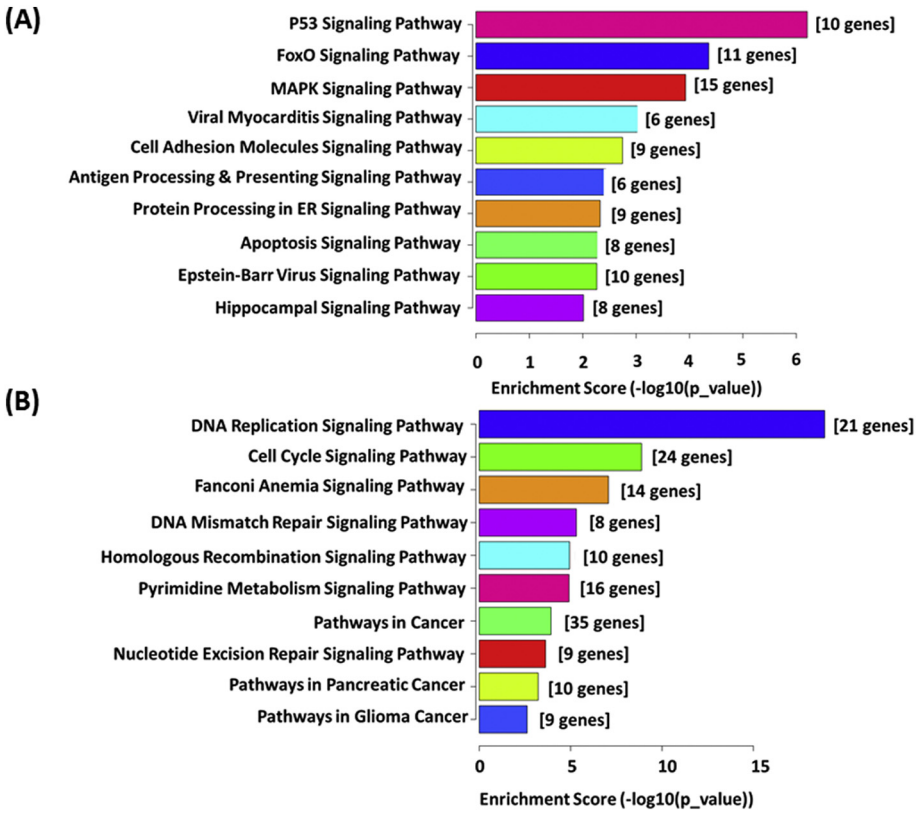

Fig. 5. The top 10 significant pathways of DEGs of pEV control samples versus pmiR-203 stable U251 cell samples based on the latest KEGG database. (A) represents the top 10 significantly altered pathways of control versus downregulated DEGs. (B) represents the top 10 significantly altered pathways of control versus upregulated DEGs. The analysis allows users to determine whether the DEGs are enriched in certain biological pathways. The *p-values* ($p \leq .05$) calculated by Fisher's exact test is used to estimate the statistical significance of the enrichment of the pathways between the pEV control versus pmiR-203 treated U251 cells.

Table 3
Shows top 20 significantly differential skipped exon (SE) splicing analysis of miR-203 expressing stable U251 cells compared to control samples.

SEID	Gene Name	Gene ID	Skipped Exon Event	Splicing Ratio	Coverage1	Coverage2	DE_Fold_Change	DE_p_value
15,802	ENSG00000136861	chr9 - CDK5RAP2	ENSG00000136861_123205898_123206020	0.679110506	40.1803279	2.53005464	0.092168691	0.00E + 00
31,392	ENSG00000128595	chr7 + CALU	ENSG00000128595_128407510_128407709	1.364399535	352.60804	56.6951424	0.140419872	0.00E + 00
27,621	ENSG00000171130	chr7 + ATP6V0E2	ENSG00000171130_149575767_149575835	1.217896799	36.1029412	91.1029412	1.571682054	0.00E + 00
1566	ENSG00000106665	chr7 + CLIP2	ENSG00000106665_73787262_73787366	2.396808764	2.69230769	15.0128205	1.63855583	0.00E + 00
38,848	ENSG00000013561	chr5 + RNF14	ENSG00000013561_141354369_141354520	1.22169718	76.1986755	16.1743929	0.171539115	0.00E + 00
38,914	ENSG00000135540	chr6 - NHSL1	ENSG00000135540_138763120_138763251	1.6991539	5.24936387	13.7480916	1.594648152	0.00E + 00
40,592	ENSG00000112031	chr6 - MTRF1L	ENSG00000112031_153312320_153312456	0.723020592	22.1519608	5.21568627	0.286861244	0.00E + 00
40,595	ENSG00000112031	chr6 - MTRF1L	ENSG00000112031_153312320_153312551	0.710407679	17.9264069	4.05916306	0.286861244	0.00E + 00
13,993	ENSG00000114491	chr3 + UMPS	ENSG00000114491_124453940_124454093	0.758786566	108.647059	17.4052288	0.209451159	0.00E + 00
16,084	ENSG00000163694	chr4 - RBM47	ENSG00000163694_40438458_40438664	1.45101393	57.02589	22.2686084	0.258085956	0.00E + 00
13,836	ENSG00000170390	chr4 + DCLK2	ENSG00000170390_151174626_151174708	2.252420803	1.59349593	12.5772358	3.66854074	0.00E + 00
27,405	ENSG00000100281	chr22 + HMGXB4	ENSG00000100281_35659975_35660089	1.328115569	14.5233918	3.55847953	0.159198572	0.00E + 00
33,805	ENSG00000134686	chr1 - PHC2	ENSG00000134686_33791396_33791562	0.785631283	6.69477912	11.1686747	2.359372749	0.00E + 00
43,121	ENSG00000143393	chr1 - PI4KB	ENSG00000143393_151297221_151297393	1.761165651	11.4748062	50.1976744	2.469888066	0.00E + 00
13,368	ENSG00000160685	chr1 + ZBTB7B	ENSG00000160685_154986491_154986569	1.889914193	16.7222222	112.521368	3.839990388	0.00E + 00
22,654	ENSG00000117335	chr1 + CD46	ENSG00000117335_207958964_207959027	1.417241945	155.47619	27.6666667	0.591315513	0.00E + 00
11,423	ENSG00000071051	chr2 + NCK2	ENSG00000071051_106497784_106498505	1.203408793	72.4100786	39.6278317	0.524123814	0.00E + 00
6971	ENSG00000148737	chr10 + TCF7L2	ENSG00000148737_114919679_114919751	2.402362783	13.0648148	15.1944444	0.781499926	0.00E + 00
6975	ENSG00000148737	chr10 + TCF7L2	ENSG00000148737_114920378_114920450	2.993127829	8.07407407	13.6666667	0.90125961	0.00E + 00

[Abbreviation: SEID: ID of Skipped Exon candidate event when extracting from annotation file; DE: Differential Expression].

(50 mM/ml Tris-HCL pH 8.0, 150 mM/ml NaCl, 1% sodium deoxycholate, 0.1% SDS) containing 1 mM sodium orthovanadate, 0.5 mM PMSF, 10 mg/ml leupeptin. The protein concentration was determined by Bradford assay [36]. Equal amounts of protein were resolved on SDS-PAGE and then subject to western transfer onto nitrocellulose membranes and kept overnight. The blots were blocked with 5% nonfat dry milk in TBST (Tris buffer saline with 0.1% Tween-20) and probed overnight with primary antibodies against BCL2, SPARC, ROBO1, AKT, PDGFA, CREB, c-JUN, Caspase-3, Caspase-7, PARP, cleaved PARP and BAX (1:1000; Santa Cruz Biotechnology, Dallas, TX), followed by incubation with species-specific HRP-conjugated secondary antibodies (1:10000; Santa Cruz Biotechnology, Dallas, TX). An Amersham™ ECL™ Prime (GE Healthcare, Piscataway, NJ) system was used to detect chemiluminescent signals. GAPDH antibody (1:2500; Santa Cruz Biotechnology, Dallas, TX) was used to verify equal amounts of proteins were loaded in all lanes. Densitometric analysis of protein bands was performed using Image J software (National Institutes of Health (NIH), Stapleton, NY, USA).

3.9. 3'-UTR Luciferase reporter assay

For luciferase reporter assay, glioma U251 and U87 cells were co-transfected with the luciferase reporter BCL2 plasmid containing 3'-UTR with mock, pEV and pmiR-203 using FuGene®HD (Roche,

Table 4
Represents top 20 significantly differential retained intron (RI) splicing analysis of miR-203 expressing stable U251 cells compared to control samples.

RIID	Gene Name	Gene ID	Retained Intron Event	Splicing Ratio	Coverage1	Coverage2	DE_Fold_Change	DE_p_value
1585	ENSG00000137504	chr11 - CREBZF	ENSG00000137504_85374646_85374858	0.365047414	37.814465	1.789308176	0.587260936	0.00E + 00
8993	ENSG00000148719	chr10 - DNAJB12	ENSG00000148719_74094376_74095537	1.200651658	23.060293	40.99770313	1.529022098	3.12E-274
9285	ENSG00000186501	chr1 + TMEM222	ENSG00000186501_27660773_27661869	0.746756895	9.7843674	12.33333333	1.820749543	2.32E-244
13,934	ENSG00000122952	chr10 - ZWINT	ENSG00000122952_58117947_58118137	1.754724135	15.75614	7.752631579	0.336391881	2.80E-225
6443	ENSG00000158941	chr8 + CCAR2	ENSG00000158941_22476869_22477150	0.766118515	55.59312	83.34282325	2.083975504	2.61E-219
1972	ENSG00000075624	chr7 - ACTB	ENSG00000075624_5568351_5568791	0.650795676	40.415909	56.44545455	2.196077949	1.40E-172
4123	ENSG00000197622	chr1 - CDC42SE1	ENSG00000197622_151027603_151028152	0.755962788	33.486946	64.62234366	2.649562805	3.52E-172
6081	ENSG00000147454	chr8 + SLC25A37	ENSG00000147454_23424327_23425834	0.768658143	82.465605	18.19884981	0.294434967	1.20E-169
7138	ENSG00000128159	chr22 - TUBGCP6	ENSG00000128159_50658445_50658679	0.373146503	21.790598	10.85042735	1.209254863	1.20E-169
15,991	ENSG00000166965	chr15 + RCCD1	ENSG00000166965_91500131_91500342	0.513293902	31.562401	29.94470774	2.010092104	6.98E-141
17,751	ENSG00000179335	chr15 + CLK3	ENSG00000179335_74912567_74914460	0.572646032	9.0797676	13.25532664	2.621065262	1.19E-124
16,365	ENSG00000178252	chr3 + WDR6	ENSG00000178252_49051550_49051642	0.650056631	14.043478	10.96376812	1.22416094	1.08E-123
15,121	ENSG00000166471	chr11 - TMEM41B	ENSG00000166471_9302589_9304917	0.57551847	20.508877	2.799971363	0.246654016	3.14E-123
17,581	ENSG00000102854	chr16 + MSLN	ENSG00000102854_818566_818647	1.292613085	29.123457	4.637860082	0.126204348	7.60E-123
12,443	ENSG00000008513	chr8 - ST3GAL1	ENSG00000008513_134488318_134488520	1.315007527	20.607261	12.29042904	0.468788809	1.19E-122
16,991	ENSG00000111364	chr12 + DDX55	ENSG00000111364_124092210_124093226	0.799060801	13.824803	2.397637795	0.22214853	9.32E-117
11,255	ENSG00000158828	chr1 + PINK1	ENSG00000158828_20975126_20975487	0.383562447	25.088643	32.90212373	3.357723249	1.04E-114
14,207	ENSG00000100201	chr22 - DDX17	ENSG00000100201_38884121_38888060	0.405783001	49.394601	1.798172125	0.103157056	1.36E-95
7765	ENSG00000144635	chr3 - DYNC1LI1	ENSG00000144635_32611912_32612116	1.731204966	64.183007	21.02941176	0.200455387	5.37E-91

[Abbreviation: RIID: ID of Retained Intron candidate event when extracting from annotation file; DE: Differential Expression].

Table 5
Represents top 20 significantly differential alternative 3′ splice site (A3SS) splicing analysis of miR-203 expressing stable U251 cells compared to control samples.

A3SSID	Gene Name	Gene ID	Alternative 3' Splice Site Event	Splicing Ratio	Coverage1	Coverage2	DE_Fold_Change	DE_p_value
3669	ENSG00000168036	chr3 + CTNNB1	ENSG00000168036_41281151_41281309	1.41156252	149.5801688	19.025316	0.119054667	1.32E-173
7010	ENSG00000169242	chr1 + EFNA1	ENSG00000169242_155105979_155106205	0.770124808	104.880531	315.82891	3.968445369	1.86E-109
2447	ENSG00000134644	chr1 - PUM1	ENSG00000134644_31439045_31439125	1.423805694	13.89583333	6.7916667	0.3131394	7.67E-80
4806	ENSG00000132906	chr1 - CASP9	ENSG00000132906_15833571_15833628	1.212787195	60.1871345	392.92398	5.753484241	2.86E-75
3257	ENSG00000141503	chr17 + MINK1	ENSG00000141503_4794751_4794810	1.201658398	65.2259887	131.9435	1.754122232	1.71E-72
108	ENSG00000142330	chr2 + CAPN10	ENSG00000142330_241535351_241535735	0.623075274	10.73090278	11.766493	1.834343672	3.42E-72
4585	ENSG00000126351	chr17 + THRA	ENSG00000126351_38249273_38249389	2.287262554	40.93103448	327.39655	3.083726329	3.64E-71
6781	ENSG00000109046	chr17 + WSB1	ENSG00000109046_25634770_25636125	0.786934952	10.34317343	1.6248462	0.214105837	3.27E-67
6047	ENSG00000158856	chr8 + DMTN	ENSG00000158856_21924216_21924348	0.679703428	66.32323232	212.07071	4.83652753	3.50E-64
4256	ENSG00000101040	chr20 - ZMYND8	ENSG00000101040_45927617_45927691	1.202163246	15.71621622	3.6756757	0.223609507	1.24E-55
5446	ENSG00000140854	chr16 + KATNB1	ENSG00000140854_57789702_57789752	0.770252979	25.64	45.48	2.427487595	2.27E-51
1626	ENSG00000128604	chr7 + IRF5	ENSG00000128604_128587284_128587331	0.721209052	6.219858156	12.120567	1.866444001	1.02E-49
7590	ENSG00000244257	chr16 + PKD1P1	ENSG00000244257_16412371_16412407	1.449903442	89.87962963	198.62963	1.923659526	5.45E-44
1131	ENSG00000168487	chr8 + BMP1	ENSG00000168487_22058631_22059315	0.608729221	20.24756335	26.557992	2.276703274	1.21E-43
521	ENSG00000169592	chr16 + INO80E	ENSG00000169592_30012533_30012734	0.779950351	19.84411277	22.925373	1.599730302	9.05E-43
4050	ENSG00000089159	chr12 - PXN	ENSG00000089159_120653077_120653220	1.301878452	41.8951049	180.47319	3.868883581	1.27E-42
3250	ENSG00000067141	chr15 + NEO1	ENSG00000067141_73528628_73528687	1.209229126	19.76836158	9.3276836	0.407724333	5.92E-41
679	ENSG00000064961	chr19 + HMG20B	ENSG00000064961_3574339_3574367	1.284646977	20.38095238	54.166667	2.291947126	3.61E-39
2386	ENSG00000170485	chr2 + NPAS2	ENSG00000170485_101611862_101612257	1.40299946	49.88945148	40.925738	0.631771705	1.74E-38

[Abbreviation: A3SS: ID of Alternative 3' Splice Site candidate event when extracting from annotation file; DE: Differential Expression].

Indianapolis, IN) transfection kit according to the manufacturer's instructions. Following transfection for 36 h, the luciferase activity in each group was measured using the Dual-Luciferase Reporter Assay System (Promega Corp., Madison, WI), in accordance with the manufacturer's instructions. The experiments were performed in triplicate and intensity of Renilla luciferase was normalized by firefly luciferase and the luc/Rluc-BCl2 3'UTR activity was calculated as the mean ± standard errors of the mean (SEM) after being normalized against Firefly luciferase activity.

3.10. TUNEL assay for staining of apoptotic cells

Apoptotic response was measured by using the terminal deoxynucleotide transferase (TdT)-mediated biotin-dUTP nick end labeling (TUNEL), the commercially available DeadEnd™ Fluorometric TUNEL system in situ cell death detection kit (Promega Corp, Madison, WI). This kit was used to measure the fragmented DNA in apoptotic cells by catalytically incorporating fluorescein-12–dUTP at the 3′-OH DNA ends using rTdT. Glioma U251 and U87 cells were seeded onto sterile 8-well chamber slides and transfected with mock, pEV and pmiR-203. After 36 h, cells were washed and fixed with 4% para-formaldehyde and permeabilized with 0.1% Triton X-100 for 5–7 min. Cells were then incubated with TUNEL reaction mixture for 60 min at 37 °C in a humidified chamber. After being slides were washed with three times with PBS, the sections were immersed in 40 ml of freshly prepared propidium iodide/DAPI solution (1 mg/ml) for 15 min at room temperature in the dark. The slides were washed three times with PBS and the incorporated biotin-dUTP exhibiting green fluorescence was detected under a BZ-X700 fluorescence microscope (Keyence, Osaka, Japan).

3.11. qRT-PCR validation of RNA-seq data

Total RNA was extracted from glioma cells (U251 and U87) overexpressed with miR-203 (1 and 2 μg/ml), mock or pEV controls as well as total RNA was also extracted from miR-203 expressing U251 stable cells and U251 pEV control samples for qRT-PCR RNA-seq validation analysis of 8-apoptosis related genes that were found to be significantly enriched in apoptosis signaling pathway using TRIzol® solution (Invitrogen, Carlsbad, CA) as per standard protocol. For cDNA synthesis total RNA (1 μg) was reverse transcribed with high-capacity cDNA reverse transcription kit (Applied Biosystems, Foster City, CA), and subsequently used to amplify BCL2, SPARC, AKT, ROBO1, PDGFA, CREB,

Table 6
Represents top 20 significantly differential alternative 5′ splice site (A5SS) splicing analysis of miR-203 expressing stable U251 cells compared to control samples.

A5SSID	Gene Name	Gene ID	Alternative 5' Splice Site Event	Splicing Ratio	Coverage1	Coverage2	DE_Fold_Change	DE_p_value
1608	ENSG00000059145	chr16 - UNKL	ENSG00000059145_1417093_1417242	1.398091958	40.01118568	21.606264	0.488565073	0.00E + 00
4992	ENSG00000167193	chr17 - CRK	ENSG00000167193_1339914_1340083	1.31454453	27.89546351	4.321499	0.100247128	0.00E + 00
1992	ENSG00000168101	chr16 + NUDT16L1	ENSG00000168101_4744240_4744309	1.530065585	24.81642512	71.338164	2.077995385	4.17E-232
3292	ENSG00000132256	chr11 - TRIM5	ENSG00000132256_5706098_5706245	0.765966459	15.10884354	4.5736961	0.401696712	4.03E-149
4550	ENSG00000185504	chr17 - C17orf70	ENSG00000185504_79518758_79518953	1.435078117	21.51623932	44.965812	1.619310781	2.88E-135
3578	ENSG00000099364	chr16 + FBXL19	ENSG00000099364_30939821_30939949	0.68504186	40.796875	61.096354	1.624422445	5.38E-133
5132	ENSG00000179335	chr15 + CLK3	ENSG00000179335_74912567_74914557	0.758634176	17.45477387	33.796985	2.641956832	2.49E-128
530	ENSG00000156253	chr21 - RWDD2B	ENSG00000156253_30380561_30380715	0.72158042	26.38961039	4.9848485	0.275331043	4.27E-125
1074	ENSG00000154040	chr18 + CABYR	ENSG00000154040_21736007_21736963	1.275517089	15.93549512	12.844142	0.665423131	3.71E-120
1461	ENSG00000164967	chr9 - RPP25L	ENSG00000164967_34611857_34612060	1.25348445	74.77832512	141.5353	1.554992833	7.87E-119
2723	ENSG00000144381	chr2 - HSPD1	ENSG00000144381_198363399_198363445	1.202876389	26.52898551	4.7391304	0.157628703	3.85E-109
3631	ENSG00000198074	chr7 + AKR1B10	ENSG00000198074_134223770_134223827	1.319017359	17,195.73684	11,066.789	0.571714659	1.78E-84
4278	ENSG00000128973	chr15 - CLN6	ENSG00000128973_68503894_68504012	0.696334718	31.78531073	30.514124	1.490279122	2.13E-66
4280	ENSG00000128973	chr15 - CLN6	ENSG00000128973_68503987_68504012	0.747922363	23.18666667	23.88	1.490279122	2.13E-66
4086	ENSG00000077235	chr16 - GTF3C1	ENSG00000077235_27475641_27475715	0.718424808	40.49099099	45.756757	1.346904965	5.98E-63
1249	ENSG00000156482	chr8 - RPL30	ENSG00000156482_99057055_99057170	0.584334533	241.7101449	49.695652	0.356970618	7.65E-62
678	ENSG00000118181	chr11 - RPS25	ENSG00000118181_118888635_118888667	0.797750715	46.15625	13.8125	0.404185456	3.76E-57
1703	ENSG00000148187	chr9 + MRRF	ENSG00000148187_125027825_125028059	0.589241475	33.19373219	6.5911681	0.284596967	1.93E-54
4722	ENSG00000107815	chr10 + C10orf2	ENSG00000107815_102750768_102750811	1.226171957	80.87596899	80.627907	0.929702518	7.01E-47
593	ENSG00000243716	chr16 + NPIPB5	ENSG00000243716_22530591_22530735	0.621113266	35.31481481	9.912037	0.399178637	2.03E-43
4279	ENSG00000128973	chr15 - CLN6	ENSG00000128973_68503894_68503986	0.627144052	17.29710145	14.942029	1.488230827	8.21E-43
2868	ENSG00000130734	chr19 + ATG4D	ENSG00000130734_10657748_10657791	0.750164496	6.550387597	17.48062	3.57800966	2.95E-41

[Abbreviation: A5SS: ID of Alternative 5' Splice Site candidate event when extracting from annotation file; DE: Differential Expression].

c-JUN as well as 8-apotosis related differentially expressed genes found to be significantly enriched in apoptosis signaling pathway from our RNA-seq data and were validated using qRT-PCR analysis and these genes were BCL2L11, BBC3, DDIT3, GADD45A, GADD45B, DFFB, EIF2AK3 and TUBA4A (primer sequences of these 8 genes as well as miR-203 predicted 7 target genes are presented in Supplementary Material, Table S1). All of these genes were amplified using iTaq™ Universal SYBR® Green Supermix kit (Bio-Rad Laboratories, Hercules, CA). GAPDH was used as a housekeeping reference gene in this analysis. qRT-PCR reaction mix was performed and primers for qRT-PCR were synthesized using the CFX96™ Real-Time PCR System (Bio-Rad Laboratories, Hercules, CA). Fold changes between the pmiR-203 and the control group (mock or pEV) were calculated using delta-delta cycle threshold (ΔΔCt) values and normalized with *GAPDH* as a housekeeping gene. Statistical significance of the transcript levels between pmiR-203 versus the control group was calculated using an unpaired *t*-test in GraphPad Prism 5 Software (GraphPad Software Inc., San Diego, CA).

3.12. Statistical analysis

At least three independent experiments were performed in triplicate, and data were present as the mean ± standard errors of the mean (SEM). The significance of difference between different treatment groups was analyzed using student's *t*-test or a one-way analysis of variance (ANOVA). For all analyses, the level of significance was set at $p < .05$ (*) and $p < .01$ (**). Principal component analysis (PCA) and correlation analysis were based on gene expression level, Heat map (Hierarchical clustering), Gene Ontology (GO), biological pathway analysis, scatter and volcano plots were performed with differentially expressed genes in R software 3.4.1 and python 2.7.

4. Results

4.1. Overexpression of miR-203 in glioma cells

To examine the potential role of miR-203 in GBM, we examined the miR-203 expression level in glioma cell lines and we found that the miR-203 expression was very low in U251 and U87 cells compared to human astrocytes cells (Fig. 1A). In addition, we have previously shown that miR-203 expression was at especially low levels in GBM tissue compared to normal brain tissue [23]. miR-203 plays an essential role in glioma cell proliferation, migration and sensitivity to induction of apoptosis. To experiment with a genetic approach to induce miR-203 expression and observe its effects on GBM tumor growth in vitro, we cloned a human precursor miR-203 (has-miR-203) cDNA in a phCMV-C-Luc mammalian expressing vector and transfected it into U251, U87 parental (U251−P and U87−P) cells. The stable cell lines over-expressing miR-203 were designated as U251-SP and U87-SP, whereas the stable cell lines expressing the empty vector (phCMV-C-Luc) was designated as U251-EV and U87-EV. We randomly tested clones for mRNA expression of miR-203 transcript and selected five clones and determined the levels of miR-203 using qRT-PCR. There were a more than threefold increase in miR-203 transcript levels in U251-SP, U87-SP clones (U251-SP1 to SP5 and U87-SP1 to SP5; $p < .01$ compared to controls; Fig. 1B and C). We next examined the miR-203 expression levels in patients with high and low grade glioma to evaluate the role of miR-203 expression on the survival rate of brain tumor patients in the Human Cancer Genome Atlas (TCGA) database [37]. We observed that miR-203 expression was high in patients with low grade glioma (LGG) compared to patients with high grade glioma (GBM). As shown in Fig. 1D, high miR-203 expressing low grade glioma (LGG) patients had significantly 2-to-3 fold longer survival as compared to patients expressing low levels of miR-203 in 3-to-5-year relative survival rate (HR = 0.92, 95% CI 0.85–1.0; $p < .05$).

4.2. Differentially expressed genes screening from high-throughput RNA-seq

We performed next high-throughput RNA-sequencing in miR-203 overexpressing stable cells to identify novel genes, transcripts, pathways and biological functions associated with miR-203 GBM pathophysiology. The expression profile data were firstly preprocessed and then analyzed using R and Python statistical packages and the bioinformatics workflow was shown in Supplementary Material, Fig. S1. A total of 1192 differentially expressed genes, 847 up-regulated and 345 downregulated, were identified in miR-203 expressing U251 stable cells compared with their U251-EV control cells ($p \leq .05$, *q-values* ≤ 1 (FDR adjusted *p-values)*) (Supplementary Material, Table S2). Using the unsupervised hierarchical clustering heatmap shows a very remarkable clustering pattern of differentially expressed genes in one dimensional clustering pattern across miR-203 stable U251 cells and U251-EV control cells (Fig. 2A and B). In addition, we also identified a total of 8269 novel genes (Supplementary Material, Table S3) and a total of

Table 7
Represents top 20 significantly differential Mutually Exclusive Exons (MXEs) splicing analysis of miR-203 expressing stable U251 cells compared to control samples.

MXEID	Gene Name	Gene ID	Mutually Exclusive Exons Event	Splicing Ratio	Coverage1	Coverage2	DE_Fold_Change	DE_p_value
1139	ENSG00000096063	chr6 - SRPK1	ENSG00000096063_35806114_35806206_35806483_35806575	13.33998143	19.78985507	2.304347826	0.132876168	0.00E + 00
588	ENSG00000148737	chr10 + TCF7L2	ENSG00000148737_114919679_114919751_114920378_114920450	3.038726977	13.06481481	15.19444444	0.781499926	0.00E + 00
2679	ENSG00000100528	chr14 - CNIH1	ENSG00000100528_54896979_54897122_54898826_54898938	1.33136303	640.5827506	223.4638695	0.330963766	3.31E-235
908	ENSG00000091409	chr2 + ITGA6	ENSG00000091409_173335702_173335833_173337502_173337618	8.442064658	13.67684478	4.384223919	0.124551198	6.03E-202
772	ENSG00000087903	chr19 - RFX2	ENSG00000087903_6042055_6042134_6044204_6044293	1.641479465	5.17721519	14.10126582	2.324903887	1.61E-139
641	ENSG00000100814	chr14 - CCNB1IP1	ENSG00000100814_20785953_20786133_20786415_20786629	2.282114447	13.70185185	10.63148148	0.373675952	5.82E-118
642	ENSG00000100814	chr14 - CCNB1IP1	ENSG00000100814_20785954_20786133_20786415_20786629	2.282114447	13.68528864	10.62383613	0.373675952	5.82E-118
3199	ENSG00000182473	chr17 - EXOC7	ENSG00000182473_74086410_74086478_74087224_74087316	0.748065038	33.54901961	41.98039216	1.815652769	2.54E-111
2144	ENSG00000142192	chr21 - APP	ENSG00000142192_27369675_27369731_27372330_27372497	1.203047123	60.9702381	7.696428571	0.231984863	4.88E-108
2382	ENSG00000159023	chr1 + EPB41	ENSG00000159023_29424319_29424447_29435848_29435949	1.347191035	25.72135417	3.809895833	0.092578971	4.12E-94
2044	ENSG00000138698	chr4 + RAP1GDS1	ENSG00000138698_99264290_99264412_99273627_99273752	1.773117484	42.53005464	10.94535519	0.229515256	1.95E-93
3305	ENSG00000050748	chr5 - MAPK9	ENSG00000050748_179674439_179674510_179674855_179674926	2.103040568	86.53521127	7.788732394	0.255774121	3.08E-91
3250	ENSG00000175662	chr17 - TOM1L2	ENSG00000175662_17786019_17786177_17787948_17788082	0.758932593	28.21308017	91.73839662	5.231128415	4.24E-91
2845	ENSG00000166411	chr15 + IDH3A	ENSG00000166411_78449890_78449973_78452434_78452548	1.45992197	97.10441767	35.29718876	0.257927143	6.24E-89
1591	ENSG00000122882	chr10 - ECD	ENSG00000122882_74912051_74912179_74914014_74914206	1.200478772	17.24479167	2.026041667	0.214636534	9.06E-85
3916	ENSG00000125944	chr1 - HNRNPR	ENSG00000125944_23650049_23650225_23660011_23660124	1.369123852	159.1666667	34.70075758	0.141969559	1.68E-82
500	ENSG00000137814	chr15 + HAUS2	ENSG00000137814_42850396_42850488_42851537_42851606	0.523036325	13.79710145	2.760869565	0.30904568	2.41E-78
1053	ENSG00000119787	chr2 - ATL2	ENSG00000119787_38570410_38570654_38581209_38581319	1.859803172	31.72404372	5.084699454	0.261853783	6.66E-71
240	ENSG00000066427	chr14 - ATXN3	ENSG00000066427_92555074_92555161_92562437_92562481	6.003379339	10.7164751	2.363984674	0.196251119	3.09E-67

[Abbreviation: MXEID: ID of Mutually Exclusive Exons candidate event when extracting from annotation file; DE: Differential Expression].

12,086 novel transcripts (Supplementary Material Table S4) in U251 miR-203 stable cells versus U251-EV control samples from whole transcriptome RNA-seq data. The top 25 significantly up-regulated differentially expressed genes and down-regulated differentially expressed genes are shown in Table 1 and Table 2 according to fold change (FC).

4.3. Functional enrichment analysis

In order to make functional interpretation for the gene expression changes, we performed GO analysis based on Fisher's exact test. Functional enrichment analysis was performed for all differentially expressed genes. The result revealed significant enrichment of upregulated and downregulated differentially expressed genes in GO analysis and were classified based on their functional enrichment in three different categories: biological process (BP), cellular component (CC) and molecular function (MF) ($p < .05$) from the miR-203 stable U251 cells versus U251-EV control samples. In the enrichment analysis of GO category of BP, we observed the highest enrichment related to negative regulation of cellular proliferation, apoptosis process, cell adhesion, regulation of cell death etc., in downregulated differentially expressed genes (Fig. 3A) whereas in upregulated differentially gene express showed the highest enrichment of category related to DNA replication, DNA replication initiation and cell division (Fig. 4A) etc. In the enrichment analysis of GO category of molecular function (MF), we observed the highest enrichment of category related to protein binding, identical protein binding, calcium ion binding, cadherin binding and transcription factor binding in downregulated differentially expressed genes (Fig. 3C), whereas protein binding, single stranded DNA dependent ATP activity and histone binding were significantly found to be enriched in GO category of MF of up-regulated differentially expressed genes (Fig. 4C). The GO analysis in the cellular component category identified the highest enrichment related to nucleus, cytosol, plasma membrane, cytoplasm, golgi membrane and extracellular exosome, nucleoplasm, condensed chromosome kinetochore in up and down regulated genes (Fig. 3B and 4B). GO functional enrichment analysis revealed profound deregulation in three core processes by miR-203 in glioma U251 cells compared to U251-EV control cells: negative regulation of cell proliferation, apoptosis, cell death, DNA replication and cell cycle regulation. All of these three processes identified as hallmarks of human cancer [38] and observed widespread alteration in the miR-203 overexpressed transcriptome suggesting a driver role of miR-203 in brain cancer tumorigenesis.

4.4. Biological pathway analysis of differentially expressed genes

We performed pathway analysis using the latest KEGG database in order to understand which signaling pathways were altered in miR-203 U251 stable cells compared to U251-EV control cells. We used upregulated and downregulated differentially expressed genes to identify top enriched biological pathways associated with miR-203 stable U251 cells versus U251 EV control samples. Our results showed a total 36 pathways were significantly altered in upregulated differentially expressed genes, whereas a total of 23 pathways were significantly altered in downregulated differentially expressed genes. Fig. 5A and B shows top 10 statistically significant enriched biological pathways associated with up and downregulated differentially expressed genes ($p < .05$). As shown in Fig. 5A, the main biological pathways implicated in downregulated differentially expressed genes were p53 signaling pathway, FoxO signaling pathway, MAPK signaling pathway, viral myocarditis signaling pathway, cell adhesion molecule signaling pathway, antigen processing and presentation signaling pathway, protein processing in endoplasmic reticulum signaling pathway, apoptosis signaling pathway, Epstein Barr virus infection signaling pathway, and Hippo signaling pathway. Whereas DNA replication signaling pathway, cell cycle signaling pathway, Fanconi

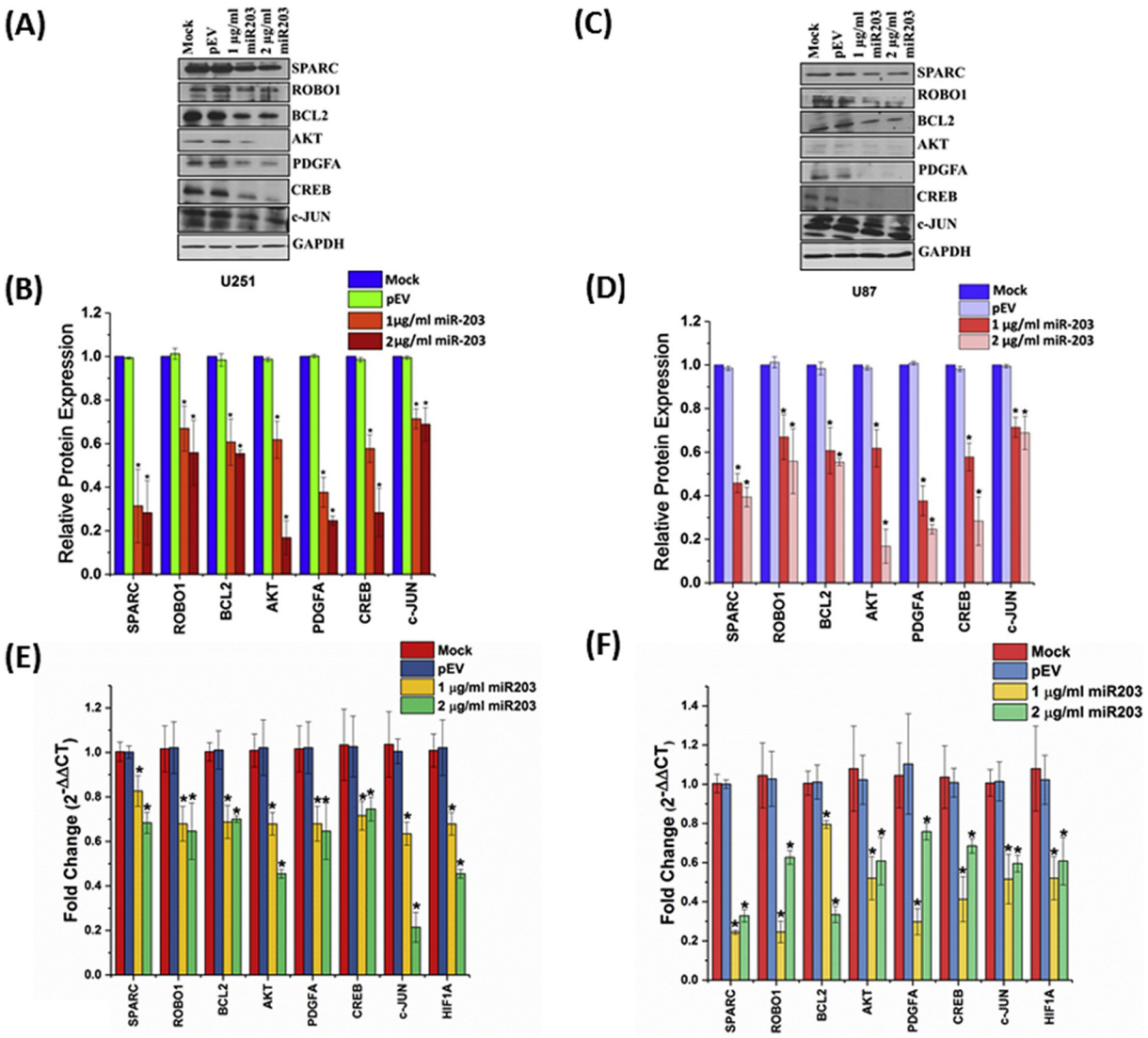

Fig. 6. The effects of enforced miR-203 expression on predicted target genes in glioma cells. U251 cells were transfected with mock or pEV or pmiR-203 for 36 h and analyzed for (A) and (B) pmiR-203 targets protein levels by western blots, and GAPDH was used as loading control. U87 cells were transfected with Mock or pEV or pmiR-203 for 36 h and analyzed for (C) and (D) pmiR-203 targets protein levels by western blots, and GAPDH was used as loading control (Mean ± SEM, $n = 3$). $^*p < .05$ vs. normal control samples. (E) U251 cells and (F) U87 cells were transfected with mock or pEV or pmiR-203 for 36 h and analyzed for gene expression levels of miR-203 predicted targets genes by qRT-PCR along with GAPDH endogenous control for normalization (Mean ± SEM, $n = 3$). $^*p < .05$ vs. normal control samples.

anemia signaling pathway, mismatch repair signaling pathway, homologous recombination signaling pathway, pyrimidine metabolism signaling pathway, pathways in cancer, nucleotide excision repair signaling pathway, pancreatic signaling pathway and glioma signaling pathway were found to be enriched with upregulated differentially expressed genes (Fig. 5B). As for the downregulated differentially expressed genes, they were mostly enriched in the induction of apoptosis via p53 signaling pathway was found to be highly significant in the topmost list of an enriched biological pathway. Whereas, in contrast, DNA replication and cell cycle signaling were found to be significantly enriched in topmost list in the upregulated differentially expressed genes, suggesting the regulation of cell cycle and disorders in DNA metabolic process counterbalance between antiapoptosis and proapoptosis related genes in response to miR-203 induction in glioma cells compared to control cells.

Gene set enrichment analysis was also performed based on the miR-203 modulating a set of differentially expressed genes compared to control samples. Enrichment plots of GSEA showed that the gene signature of G1/S transition of the mitotic cell cycle and apoptosis signaling related genes were enriched in miR-203 expressing U251 cells compared to control samples (Supplementary Material, Fig. S3). These data suggest that miR-203 may be a crucial modulator in GBM tumor progression and glioma cell tumorigenesis.

Taken together, we observed that miR-203 expression may regulate tumor progression and therapy resistance in GBM patients by modulating genes involved in p53 signaling, cell cycle regulation, DNA replication and DNA mismatch repair in pre and post apoptosis process.

4.5. Detection of alternative splicing events

Next, we performed alternative splicing analysis from RNA-seq high-throughput data based on HISAT2 alignments with human reference transcriptome GRCh37.75 (hg19) in ENSEMBL. We have used dSpliceType approach [35] to defect various types of differential splicing and differential expression events between miR-203 expressing U251 stable cells and control samples. We identified 5 most common types of splicing events including skipped exon (SE), retained intron (RI), alternative 3′ splice sites (A3SS), alternative 5′ splice sites (A5SS),

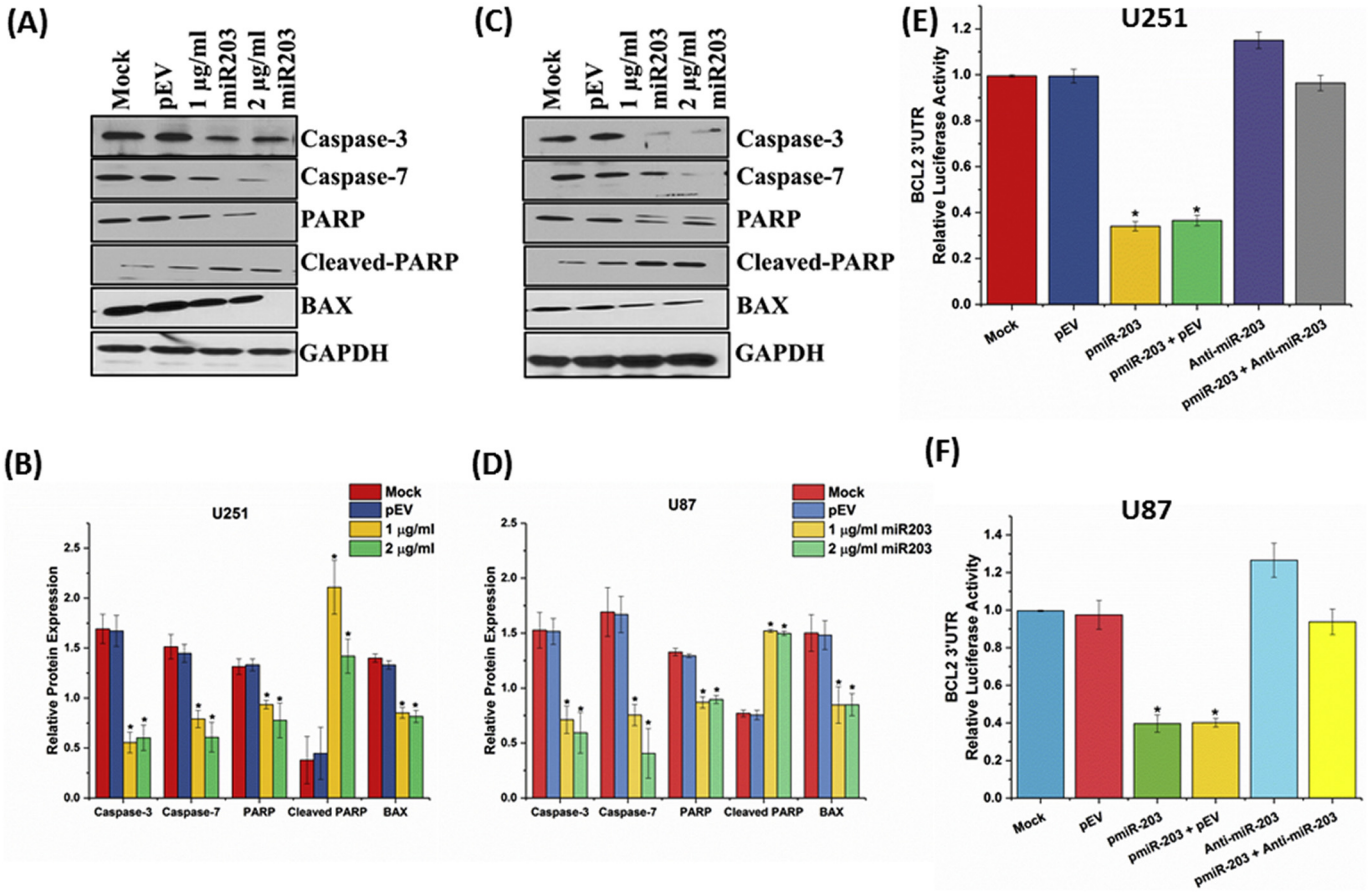

Fig. 7. The expression level of apoptosis regulated protein marker in miR-203 overexpressed glioma cells and miR-203 directly targets BCL2 in glioma cells apoptosis. U251 cells and U87 cells were transfected with mock or pEV or pmiR-203 for 36 h and analyzed for apoptosis-related protein levels in miR-203 overexpressed glioma cells with GAPDH endogenous control for normalization (Mean ± SEM, $n = 3$). (A) and (B) protein expression level of caspase-3, caspase-7, PARP, cleaved-PARP, and BAX in U251 overexpressed glioma cells compared to control samples. (C) and (D) protein expression level of caspase-3, caspase-7, PARP, cleaved-PARP, and BAX in U87 overexpressed glioma cells compared to control samples. Experiments are representatives of three biological replicates (Mean ± SEM, n = 3). $^{*}p < .05$ vs. normal control samples. (E) and (F) U251 and U87 cells were transfected with pLuc-BCL2 3'UTR reporter renilla plasmid, renilla luciferase control reporter plasmid together with Mock or pEV or pmiR-203 or Anti-miR-203 or pmiR-203 + Anti-miR-203 and measure luciferase activity after 24 h after treatment. Renilla luciferase activity was normalized by firefly luciferase (Fluc) activity (Mean ± SEM, n = 3). $^{*}p < .05$ vs. normal control samples.

and mutually exclusive exons (MXE) and filtered these splicing events based on spicing ratio and differential expression *p-value* ($p < .05$). Transcriptome analysis revealed a number of significantly differentially spliced events for miR-203 expressing U251 cells in comparison to control samples (Table 3-7, see Supplementary Material, Fig. S4 and Supplementary Material Table S5 for details of all the events), proving that manipulation of the splicing machinery resulted in alternating splicing isoforms. From this analysis, alternative splicing was more affected upon modulation of miR-203 in U251 cells compared to control samples, as the number of splicing event was larger for this splicing factor, in specifically for the events like SE (a total of 1540 events) and RI (a total of 317 events) compared to MXE, A3SS, and A5SS (Supplementary Material, Fig. S4). This might be due to the different roles that these splicing factors play in the spliceosome complex. In addition, we have identified novel alternative splicing isoforms like CDK5RAP2, CALU, ATP6V0E2, CLIP2, RNF14, NHSL1, MTRF1L, UMPS etc. in skipped exon (SE) events whereas alternative splice isoforms such as CREBZF, DNAJB12, TMEM222, ZWINT, CCAR2, ACTB, CDC42SE1, SLC25A37, TUBGCP6, RCCD1 etc. were identified in retained intron (RI) from our samples (Table 3, Table 4, Supplementary Material Table S5). Furthermore, CTNNB1, EFNA1, PUM1, CASP9, MINK1, CAPN10, THRA, WSB1 alternative splicing isoforms were identified in the A3SS specific event (Table 5, Supplementary Material Table S5). For A5SS and MXE splicing analysis, we identified top 20 alternative splicing isoforms such as UNKL, CRK, NUDT16L1, TRIMS, C17orf70, FBXL19, CLK3, RWDD2B, CABYR, RPP25L and SRPK1, TCF7L2, CNIH1, ITGA6, CCNB1IP1, EXOC7, APP, EPB41 respectively (see Table 6, Table 7, and Supplementary Material Table S5).

4.6. miR-203 predicted targets in GBM cells

We next determined the molecular mechanisms underlying the miR-203 mediated tumor suppressive effects in glioma cells. In addition to RNA-seq transcriptome profiling, we performed the separate analysis using the TargetScan (http://www.targetscan.org) to search for target genes of miR-203 and identified SPARC, BCL2, ROBO1, AKT, c-JUN, PDGFA and CREB which were shown to play a role in GBM tumorigenesis. Previously, we showed that ROBO1 is the direct target of miR203 and demonstrated that the miR203 modulates the glioma cell migration via ROBO1/ERK/MMP-9 signaling pathway [23]. We, therefore, determined the total protein and mRNA levels of these seven miR-203 predicted targets in glioma U251 and U87 cell lines transfected with miR-203 for 36 h. Fig. 6A-D indicates when adjusted with cells transfected with controls, western blot densitometry analysis revealed about 50 to 60% decrease in the expression of these miR-203 predicted targets in 1–2 μg/ml pmiR-203 transfected cell lines compared to pEV and mock control samples ($p < .05$). Fig. 6E and F represent that there was a 50–60% decrease in BCL2, SPARC, ROBO1,

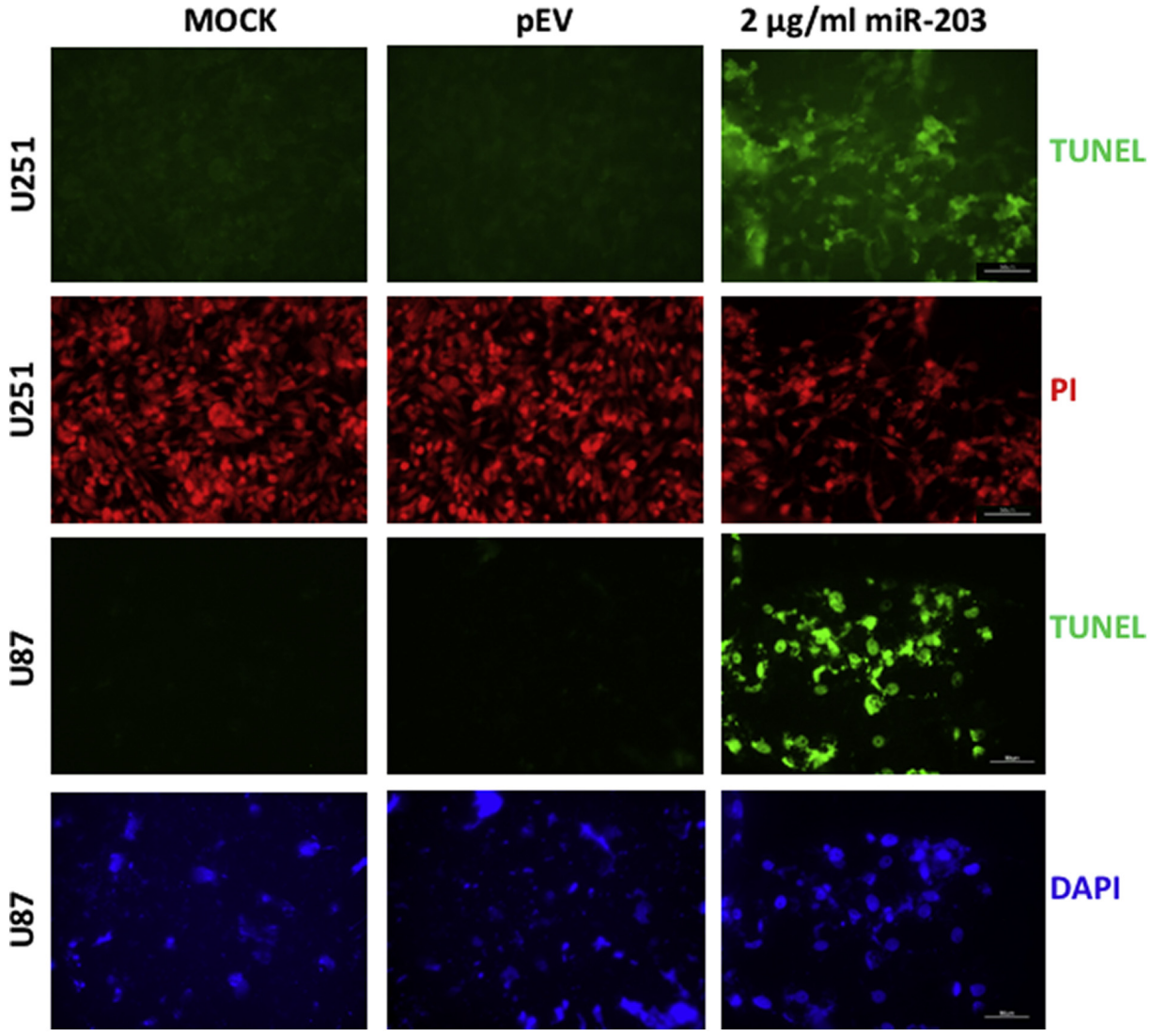

Fig. 8. miR-203 induced apoptosis in glioma cells. U251 and U87 cells were seeded in eight-well chambered slides and transfected with Mock or pEV or pmiR-203 for 36 h and after 36 h, analyzed for apoptotic response by TUNEL assay. Green fluorescent color indicates cells are undergoing in the apoptotic process and red (PI) and blue (DAPI) color staining show cells nuclei staining. Scale Bar: 50 µm. (For interpretation of the references to color in this figure legend, the reader is referred to the web version of this article.)

AKT, PDGFA, CREB and c-JUN mRNA levels in glioma U251 and U87 cells transfected with 1 and 2 µg/ml pmiR-203 compared to mock and pEV control samples ($p < .05$).

4.7. miR-203-induced apoptosis in glioma cells

Since we observed that miR-203 suppressed BCl-2 expression, we next determined whether miR-203 regulates caspase-mediated apoptotic signaling in glioma cells. In order to do that we first performed the qRT-PCR analysis of miR-203 expression level in U251 and U87 cells transfected with pmiR-203, pEV and mock control samples to confirm miR-203 overexpression. From these analyses, we showed that miR-203 expression level was significantly overexpressed compared to control samples in both glioma cell lines (Supplementary Material, Fig. S5). Further to elucidate the mechanism mediating the apoptotic effects in glioma cells, cell lysates of 1 to 2 µg/ml pmiR-203 transfected U251 and U87 cells were subjected to western blotting analysis using antibodies for caspase-3, caspase-7, BAX, and PARP. pmiR-203 transfected cells demonstrated as 50–60% decrease in total protein levels of caspase-3, caspase-7, BAX and PARP as compared to pEV and mock control samples ($p < .05$) (Fig. 7A-D). Whereas, cleaved PARP total protein level was significantly upregulated in pmiR-203 glioma cells as compared to mock and pEV control ($p < .05$).

4.8. BCL2 is a direct target of miR-203 and BCL2-mediates miR-203 induced glioma cell apoptosis

From our RNA-seq and miR-203 predicted gene target analysis, we found BCL2 is a predicted target of miR-203 as well as we also demonstrated that the gene and protein levels of BCL2 were significantly decreased in miR-203 overexpressed U251 and U87 cells compared to control samples. To analyze the molecular mechanism of miR-203 mediated apoptosis as well as to obtain further direct evidence on the role of BCL2 miR-203 mediated signaling network, we performed analysis of the putative miR-203 binding sites for the BCL2 3'UTR using luciferase assays as previously described [39]. Co-transfection of pmiR-203 (2 µg/ml) with the 2 µg/ml BCL2–3'UTR luciferase vector significantly inhibits the effect of BCL2–3'UTR luciferase activity in U251 and U87 cells compared to mock and pEV control samples ($p < .05$) (Fig. 7E and F). These results indicate that BCL2 is a direct target of miR-203 and it also suggests that the suppression of BCL2 mRNA and protein levels are specific to miR-203 mediated regulation.

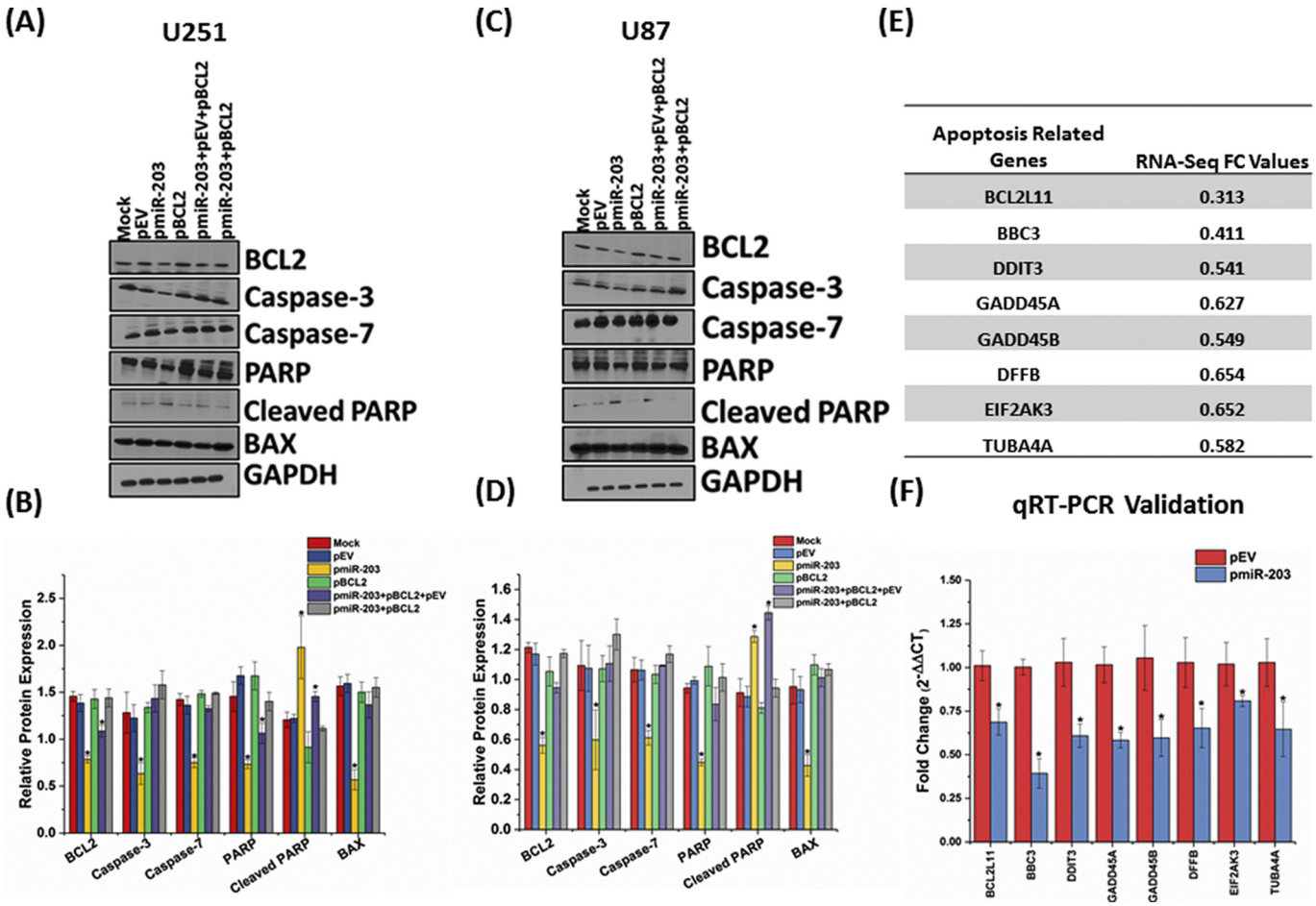

Fig. 9. BCL2 overexpression suppressed pmiR-203 induced apoptosis and qRT-PCR validation of 8 apoptotic genes were found to be significantly downregulated differentially expressed genes from RNA-seq data in miR-203 (pmiR-203) expressing U251 stable cell line compared to pEV control samples using quantitative real-time PCR (qRT-PCR). (A-D) U251 and U87 cells were transfected with Mock or pEV (2 μg/ml) or pmiR-203 (2 μg/ml) or pBCL2 (2 μg/ml) or pmiR-203 (2 μg/ml) + pEV (1 μg/ml) + pBCL2 (1 μg/ml) or pmiR-203 (2 μg/ml) + pBCL2 (2 μg/ml) for 36 h and western blotting analysis in U251 and U87 was performed for apoptotic markers (Casepae-3, Caspase-7, PARP, Cleaved-PARP and BAX) in these cells. Experiments are representatives of three biological replicates (Mean ± SEM, n = 3). *$p < .05$ vs. normal control samples. (E) The table shows 8 apoptotic genes were found to be significantly downregulated and involved in the apoptosis process and are represented by fold change (FC) values. (F) A bar graph showing 8 apoptotic genes validation using qRT-PCR. Data were normalized to GAPDH housing keeping gene. Relative expression of BCL2L11, BBC3, DDIT3, GADD45A, GADD45B, DFFB, EIF2AK3, and TUBA4A (*$p < .05$) in pmiR-203 U251 stable cells compared to empty vector (pEV) control group. Experiments are representatives of three biological replicates with duplicates (Mean ± SEM, n = 3).

Furthermore, miR-203 transfection resulted in the significantly increased number of TUNEL positive-apoptotic cells as compared pEV and mock controls (Fig. 8).

We next examined the role of BCL2 in miR-203 induced apoptosis. We transiently co-transfected U251 and U87 glioma cells with 2 μg/ml BCL2 plasmid (pBCL2) with or without 2 μg/ml pmiR-203 for 36 h and collected whole cell lysate and performed western blotting analysis to check the total protein levels. Western blotting analysis revealed that co-transfection with a plasmid expressing BCL2 reversed miR-203 mediated suppression of BCL2, caspase-3, caspase-7, PARP, BAX and cleaved PARP in pmiR-203 treated U251 and U87 glioma cells ($p < .05$) (Fig. 9A-D). Taken together, these data suggest that BCL2 activation is required for pmiR-203 mediated apoptosis in glioma cells.

4.9. qRT-PCR validation of 8-apoptosis-related genes from RNA-seq data

Our RNA-seq biological pathway analysis results revealed that apoptosis signaling pathway one of the top 10 biological pathways was found to be significantly enriched with miR-203 expression (Fig. 5A). We then next confirmed the observed changes in 8-apoptosis-related genes (BCL2L11, BBC3, DDIT3, GADD45A, GADD45B, DFFB, EIF2AK3, and TUBA4A) that were significantly enriched in the apoptosis signaling pathway using qRT-PCR. Fig. 9F demonstrates that these 8 apoptotic genes BCL2L11, BBC3, DDIT3, GADD45A, GADD45B, DFFB, EIF2AK3, and TUBA4A were significantly downregulated in miR-203 stable U251 cells compared to U251 pEV control samples ($p < .05$) (Fig. 9F). These results also aligned with observed RNA-seq fold change expression (Fig. 9E) of these 8 apoptosis-related genes.

5. Discussion

MicroRNAs (miRNAs) play critical roles in tumor progression and invasion in most of the cancers including GBM. miRNAs regulate gene and protein expression by destabilizing target mRNA or producing translational inhibition through directly binding to its 3′ untranslated region (3'UTR) of target mRNA [40]. Since it regulates multiple targets genes simultaneously, they function as the critical control nodes in the existing tumor signaling network, making them a promising target for cancer treatment. miRNAs are differentially expressed in GBM and they act variably either as oncogenes or tumor suppressor genes and aberrant expression of these miRNAs acts as a central factor for specific cancer type [15,40]. The Previous finding suggests that the roles of miRNAs in tumor malignancy have been studied via analysis of the location of specific genes for several miRNAs at sites of translocation

breakpoints or deletions linked to a specific neoplastic state [41]. Moreover, allelic deletion on chromosome 14q plays an essential role in the pathogenesis of GBM, and the site has been thought to harbor multiple tumor suppressor genes associated with GBM, a region that also encodes miR-203 [42]. Implementation of high-throughput RNA-sequencing has become a powerful tool for comprehensive characterization of the whole transcriptome at gene and exon levels and with a unique ability to identify differentially expressed genes, novel genes and transcripts, genetic variation and novel alternative splicing isoforms at high resolution and efficiency. However, till date, there were a very few miRNAs have been characterized for their specific role in cancer development, especially in glioblastoma. Hence in this study have used the high-throughput RNA-sequencing of miR-203 stable glioma cells and identified differentially expressed genes, novel transcripts, and genes, biological functions, novel alternative splicing isoforms and biological pathways. Moreover, we have also performed the separate miR-203 gene target analysis and from this analysis, we identified 7 miR-203 predicted targets and demonstrated that miR-203-induced apoptosis in glioma cells.

In this study, we focused on investigating the potential targets of GBM by analyzing the differential expression genes between miR-203 expressing glioma U251 cells compared to control samples and identified the biological functions and regulatory pathways that were altered with miR-203 expression. Previous studies determined the differentially expressed long non-coding RNAs (lncRNAs) between GBM and normal brain tissues, showing 654 up and down lncRNAs [43]. In this study, we identified a total of 1192 differentially expressed genes (847 upregulated and 345 downregulated genes) whose expression was altered in response to miR-203 compared to control samples. We then next determined biological pathway analysis and biological processes and function analysis from miR-203 expressing U251 stable cells compared to control samples. Biological function enrichment analysis shows differentially expressed genes enriched in top categories such as DNA replication, cell division, cell adhesion, cell proliferation, DNA repair, apoptosis process, angiogenesis process. These findings are consistent with the previous finding that tumor cell proliferation, cell survival, cell migration, cell invasion, angiogenesis are the key important events in malignant phenotype for a variety of cancer including GBM [44,45]. Our biological pathway analysis revealed that p53 signaling pathway, FoxO signaling pathway, MAPK signaling pathway, apoptosis signaling pathway, DNA replication, cell cycle, DNA-mismatch repair signaling pathways were altered with miR-203 expression. In addition, GSEA analysis also revealed that the gene signatures of G1/S cell cycle checkpoint and apoptosis signaling related genes were enriched in miR-203 modulated glioma cells. These were consistent with the previous finding that most of these pathways and particularly p53 signaling and MAPK signaling play an important role in GBM pathogenesis [46,47].

We also analyzed alternative splicing from our RNA-seq data of miR-203 expressing stable U251 cells compared to control samples. Previous studies have shown that changes in splicing mechanisms have been widely associated with GBM tumor malignancy. In addition, they also showed that genome-wide analysis form exon expression arrays a set of 14 genes with splicing alterations prevalent in GBM patient samples [48]. From our analysis, we have showen that several genes were differentially expressed and spliced and showed in 5 different alternative splicing categories such as SE, RI, A3SS, A5SS, and MEX. Furthermore, several of these genes were differentially expressed up and downregulated genes and may be possible act as potential GBM biomarkers.

miR-203 acts as a tumor suppressive miRNA that plays an important role in various malignancies, including pancreatic cancer, blood cancer, esophageal cancer, prostate cancer and GBM [49–52]. In addition, it was found to be down-regulated in pancreatic, esophageal cancer and gliomas, whereas in epithelial ovarian cancer it was found to be upregulated and act as an oncogene [49–52]. We previously reported using the TCGA data for high-grade glioma (HGG) that the expression of miR-203 was suppressed in these samples using qRT-PCR and in situ hybridization of glioma array. In addition, in our previous study, we have established that miR-203 was downregulated in human glioma cells, and that transfection of miR-203 suppressed glioma cell proliferation, migration, and invasiveness via targeting Robo1/ERK/MMP-9 signaling pathway [23]. In the present study, we have also determined the miR-203 expression level in glioma cell lines and we reported that miR-203 expression was found to be significantly low in glioma cells compared to normal control samples. This was consistent with previous findings that miR-203 expression levels found to be significantly lower in glioma tissue including glioblastoma, and glioma cells [19,53–56]. Here in our study, we have also demonstrated from the TCGA database analysis that miR-203 expression in lower grade glioma (LGG) overall has a better patient prognosis. There is significant variation in miR-203 expression in LGG patient samples and high miR-203 expressing patient's samples had 2 to 3-fold longer survival than low miR-203 expressing LGG human patient samples. Hence these results suggest that miR-203 can function as a prognostic biomarker in GBM.

We also show that miR-203 overexpression suppressed the total protein and gene expression of several of miR-203 predicted targets like SPARC, BCL2, ROBO1, PDGFA, AKT, c-JUN, and CREB compared to control samples. These findings are consistent with our previous finding that overexpression of miR-203 suppressed ROBO1 in glioma cells (Dontula et al., 2013). In addition, several studies have shown that overexpression of miR-203 downregulates SPARC [57], AKT, HIF-1α, and JAK in glioma cells [53]. Previous studies have shown that miR-203 expression was found to be significantly downregulated in some tumors including cancer cell lines, such as head and neck squamous cell carcinomas [58], laryngeal carcinoma cells [59], hematopoietic malignancy [60], lung carcinoma [24,61], colon cancer [21] and neuroblastoma [62]. To unravel the functional aspect of miR-203-induced glioma cell apoptosis, our studies determined that overexpression of miR-203 significantly suppressed apoptosis marker caspase-3, caspase-7, PARP, cleaved PARP, and BAX compared to control samples. Moreover, we also showed that miR-203 overexpression leads to apoptotic cell death in both U251 and U87 GBM cell lines. These findings are consistent with previous finding miR-203 overexpression induced apoptotic cell death in glioma U87 and HNGC2 cell lines using Tunnel assay [63]. Previously, it was reported that miR-203 act as a tumor suppressor in SH-SY5Y neuroblastoma cells, and overexpression of miR-203 inhibits cell proliferation and induced apoptosis in vitro and in vivo via upregulation of TGF-β1/BIM signaling [64]. Furthermore, it was shown that miR-203 overexpression inhibited in vitro glioma cell proliferation and migration, and increased sensitivity to apoptosis induced by the cytokine IFN and the chemotherapeutic agent temozolomide (TMZ) [56]. Another study revealed that ectopic expression of miR-203 sensitizes glioma cells to TMZ and it significantly inhibited glioma cell invasion via targeting E2F3 [55]. In addition, Pal et al., [63] reported that miR-203 is downregulated in glioblastoma cell lines and combats apoptosis and promote migration and proliferation potentially by targeting GAS41 in vitro.

Finally, we further investigated the mechanism of miR-203 induced apoptosis in glioma cells. Our finding report that BCL2 is a direct target of miR-203 in GBM cells and mediated miR-203 induced apoptosis. These results are consistent with the previous finding that reconstitution of miR-203 expression induced apoptosis in glioma cells [63]. There were several studies including our previous study that demonstrate that miR-203 could be a potentially useful prognostic biomarker and a therapeutic agent as the miR-203 regulatory network was shown to play an essential role in the progression and metastasis of various cancer including GBM [23,24,52]. Several studies also reported that miR-203 functioned as a tumor suppressor to control renal cell proliferation, migration, and invasion by targeting of fibroblast growth factor 2 (FGF2) in human renal cancer [65]. In addition, miR-203 overexpression inhibited cell proliferation, cell migration and invasion, and increased cell apoptosis as well as tumor growth in esophageal

cancer cells [66].

6. Conclusions

Our study reveals global functional change associated with miR-203 dysregulation in GBM cells. We observed several biological pathways that are well characterized in cancer and involved in glioma cell apoptosis, as well as GBM pathogenesis were significantly altered in miR-203 expressed cells. Additionally, we also showered that miR-203 acts as a tumor suppressor in glioma cells and it induces apoptosis via regulating BCL2.

Supplementary data to this article can be found online at https://doi.org/10.1016/j.cellsig.2018.09.014.

Acknowledgements and funding

This work was supported by the University of Illinois Cancer Center and the Division of Hematology and Oncology, Department of Medicine, UIC, IL 60612, USA.

Conflict of interest

The authors have declared that no conflict of interest exists.

Authors contributions

B.A. participated in the design of the study, performed experiments, analyzed the data and wrote the manuscripts. S.L. participated in design the study, wrote and approved the manuscript.

References

[1] H. Ohgaki, P. Kleihues, Epidemiology and etiology of gliomas, Acta Neuropathol. 109 (1) (2005) 93–108.
[2] M. Westphal, K. Lamszus, The neurobiology of gliomas: from cell biology to the development of therapeutic approaches, Nat. Rev. Neurosci. 12 (9) (2011) 495–508.
[3] S.C. Erridge, et al., Trends in classification, referral and treatment and the effect on outcome of patients with glioma: a 20 year cohort, J. Neuro-Oncol. 104 (3) (2011) 789–800.
[4] B. Pollo, Neuropathological diagnosis of brain tumours, Neurol. Sci. 32 (Suppl. 2) (2011) S209–S211.
[5] D.N. Louis, et al., The 2016 World Health Organization Classification of Tumors of the Central Nervous System: a summary, Acta Neuropathol. 131 (6) (2016) 803–820.
[6] D.N. Louis, et al., The 2007 WHO classification of tumours of the central nervous system, Acta Neuropathol. 114 (2) (2007) 97–109.
[7] M.L. Bondy, et al., Brain tumor epidemiology: consensus from the Brain Tumor Epidemiology Consortium, Cancer 113 (7 Suppl) (2008) 1953–1968.
[8] T.S. Surawicz, et al., Brain tumor survival: results from the National Cancer Data Base, J. Neuro-Oncol. 40 (2) (1998) 151–160.
[9] P.Y. Wen, S. Kesari, Malignant gliomas in adults, N. Engl. J. Med. 359 (5) (2008) 492–507.
[10] B.P. Lewis, C.B. Burge, D.P. Bartel, Conserved seed pairing, often flanked by adenosines, indicates that thousands of human genes are microRNA targets, Cell 120 (1) (2005) 15–20.
[11] W. Luo, A. Sehgal, Regulation of circadian behavioral output via a MicroRNA-JAK/STAT circuit, Cell 148 (4) (2012) 765–779.
[12] T.A. Farazi, et al., MicroRNAs in human cancer, Adv. Exp. Med. Biol. 774 (2013) 1–20.
[13] P. Liang, A.B. Pardee, Analysing differential gene expression in cancer, Nat. Rev. Cancer 3 (11) (2003) 869–876.
[14] L.A. Yates, C.J. Norbury, R.J. Gilbert, The long and short of microRNA, Cell 153 (3) (2013) 516–519.
[15] A. Esquela-Kerscher, F.J. Slack, Oncomirs - microRNAs with a role in cancer, Nat. Rev. Cancer 6 (4) (2006) 259–269.
[16] V. Profumo, P. Gandellini, MicroRNAs: cobblestones on the road to cancer metastasis, Crit. Rev. Oncog. 18 (4) (2013) 341–355.
[17] K. Boll, et al., MiR-130a, miR-203 and miR-205 jointly repress key oncogenic pathways and are downregulated in prostate carcinoma, Oncogene 32 (3) (2013) 277–285.
[18] M. Furuta, et al., miR-124 and miR-203 are epigenetically silenced tumor-suppressive microRNAs in hepatocellular carcinoma, Carcinogenesis 31 (5) (2010) 766–776.
[19] J. He, et al., MicroRNA-203 down-regulation is associated with unfavorable prognosis in human glioma, J. Surg. Oncol. 108 (2) (2013) 121–125.
[20] S. Noguchi, et al., Anti-oncogenic microRNA-203 induces senescence by targeting E2F3 protein in human melanoma cells, J. Biol. Chem. 287 (15) (2012) 11769–11777.
[21] A.J. Schetter, et al., MicroRNA expression profiles associated with prognosis and therapeutic outcome in colon adenocarcinoma, JAMA 299 (4) (2008) 425–436.
[22] Y. Yuan, et al., MicroRNA-203 inhibits cell proliferation by repressing DeltaNp63 expression in human esophageal squamous cell carcinoma, BMC Cancer 11 (2011) 57.
[23] R. Dontula, et al., MicroRNA 203 Modulates Glioma Cell Migration via Robo1/ERK/MMP-9 Signaling, Genes Cancer 4 (7–8) (2013) 285–296.
[24] C. Wang, et al., miR-203 inhibits cell proliferation and migration of lung cancer cells by targeting PKCalpha, PLoS One 8 (9) (2013) e73985.
[25] H. Liao, et al., MiR-203 downregulation is responsible for chemoresistance in human glioblastoma by promoting epithelial-mesenchymal transition via SNAI2, Oncotarget 6 (11) (2015) 8914–8928.
[26] D. Kim, B. Langmead, S.L. Salzberg, HISAT: a fast spliced aligner with low memory requirements, Nat. Methods 12 (4) (2015) 357–360.
[27] M. Martin, Cutadapt removes adapter sequences from high-throughput sequencing reads, Bioinformatics 17 (1) (2010) 10–12.
[28] M. Pertea, et al., Transcript-level expression analysis of RNA-seq experiments with HISAT, StringTie and Ballgown, Nat. Protoc. 11 (9) (2016) 1650–1667.
[29] M. Pertea, et al., StringTie enables improved reconstruction of a transcriptome from RNA-seq reads, Nat. Biotechnol. 33 (3) (2015) 290–295.
[30] J. Fu, A.C. Frazee, L. Collado-Torres, A.E. Jaffe, J.T. Leek, ballgown: Flexible, isoform-level differential expression analysis, R package version 2.6.0. (2016).
[31] A. Mortazavi, et al., Mapping and quantifying mammalian transcriptomes by RNA-Seq, Nat. Methods 5 (7) (2008) 621–628.
[32] A.C. Frazee, et al., Ballgown bridges the gap between transcriptome assembly and expression analysis, Nat. Biotechnol. 33 (3) (2015) 243–246.
[33] L. Wang, et al., CPAT: Coding-Potential Assessment Tool using an alignment-free logistic regression model, Nucleic Acids Res. 41 (6) (2013) e74.
[34] R. Edgar, M. Domrachev, A.E. Lash, Gene Expression Omnibus: NCBI gene expression and hybridization array data repository, Nucleic Acids Res. 30 (1) (2002) 207–210.
[35] D. Zhu, N. Deng, C. Bai, A generalized dSpliceType framework to detect differential splicing and differential expression events using RNA-Seq, IEEE Trans Nanobioscience 14 (2) (2015) 192–202.
[36] M.M. Bradford, A rapid and sensitive method for the quantitation of microgram quantities of protein utilizing the principle of protein-dye binding, Anal. Biochem. 72 (1976) 248–254.
[37] Cancer Genome Atlas Research, N, Comprehensive genomic characterization defines human glioblastoma genes and core pathways, Nature 455 (7216) (2008) 1061–1068.
[38] D. Hanahan, R.A. Weinberg, Hallmarks of cancer: the next generation, Cell 144 (5) (2011) 646–674.
[39] G.M. Borchert, W. Lanier, B.L. Davidson, RNA polymerase III transcribes human microRNAs, Nat. Struct. Mol. Biol. 13 (12) (2006) 1097–1101.
[40] D.P. Bartel, MicroRNAs: genomics, biogenesis, mechanism, and function, Cell 116 (2) (2004) 281–297.
[41] A. Lagana, et al., Variability in the incidence of miRNAs and genes in fragile sites and the role of repeats and CpG islands in the distribution of genetic material, PLoS One 5 (6) (2010) e11166.
[42] J. Hu, et al., High-resolution genome-wide allelotype analysis identifies loss of chromosome 14q as a recurrent genetic alteration in astrocytic tumours, Br. J. Cancer 87 (2) (2002) 218–224.
[43] L. Han, et al., LncRNA pro fi le of glioblastoma reveals the potential role of lncRNAs in contributing to glioblastoma pathogenesis, Int. J. Oncol. 40 (6) (2012) 2004–2012.
[44] S.C. Gupta, et al., Regulation of survival, proliferation, invasion, angiogenesis, and metastasis of tumor cells through modulation of inflammatory pathways by nutraceuticals, Cancer Metastasis Rev. 29 (3) (2010) 405–434.
[45] E.M. Reddy, et al., Dlxin-1, a member of MAGE family, inhibits cell proliferation, invasion and tumorigenicity of glioma stem cells, Cancer Gene Ther. 18 (3) (2011) 206–218.
[46] O.O. Kanu, et al., Glioblastoma multiforme: a review of therapeutic targets, Expert Opin. Ther. Targets 13 (6) (2009) 701–718.
[47] J.R.D. Pearson, T. Regad, Targeting cellular pathways in glioblastoma multiforme, Signal Transduct Target Ther 2 (2017) 17040.
[48] H.C. Cheung, et al., Global analysis of aberrant pre-mRNA splicing in glioblastoma using exon expression arrays, BMC Genomics 9 (2008) 216.
[49] N. Benaich, et al., Rewiring of an epithelial differentiation factor, miR-203, to inhibit human squamous cell carcinoma metastasis, Cell Rep. 9 (1) (2014) 104–117.
[50] J.H. He, et al., hsa-miR-203 enhances the sensitivity of leukemia cells to arsenic trioxide, Exp Ther Med 5 (5) (2013) 1315–1321.
[51] Z.G. Ren, et al., miR-203 promotes proliferation, migration and invasion by degrading SIK1 in pancreatic cancer, Oncol. Rep. 35 (3) (2016) 1365–1374.
[52] S. Saini, et al., Regulatory Role of mir-203 in Prostate Cancer Progression and Metastasis, Clin. Cancer Res. 17 (16) (2011) 5287–5298.
[53] J.H. Chang, et al., MicroRNA-203 Modulates the Radiation Sensitivity of Human Malignant Glioma Cells, Int. J. Radiat. Oncol. Biol. Phys. 94 (2) (2016) 412–420.
[54] Z. Chen, et al., MicroRNA-203 inhibits the proliferation and invasion of U251 glioblastoma cells by directly targeting PLD2, Mol. Med. Rep. 9 (2) (2014) 503–508.
[55] G. Tang, et al., MiR-203 sensitizes glioma cells to temozolomide and inhibits glioma cell invasion by targeting E2F3, Mol. Med. Rep. 11 (4) (2015) 2838–2844.
[56] C.H. Yang, et al., MiRNA203 suppresses the expression of protumorigenic STAT1 in glioblastoma to inhibit tumorigenesis, Oncotarget 7 (51) (2016) 84017–84029.

[57] T. Liu, et al., Bufalin Inhibits Cellular Proliferation and Cancer Stem Cell-Like Phenotypes via Upregulation of MiR-203 in Glioma, Cell. Physiol. Biochem. 44 (2) (2017) 671–681.
[58] A.M. Lena, et al., miR-203 represses 'stemness' by repressing DeltaNp63, Cell Death Differ. 15 (7) (2008) 1187–1195.
[59] K. Bian, et al., MicroRNA-203 leads to G1 phase cell cycle arrest in laryngeal carcinoma cells by directly targeting survivin, FEBS Lett. 586 (6) (2012) 804–809.
[60] M.J. Bueno, et al., Genetic and epigenetic silencing of microRNA-203 enhances ABL1 and BCR-ABL1 oncogene expression, Cancer Cell 13 (6) (2008) 496–506.
[61] N. Wang, et al., miR-203 suppresses the proliferation and migration and promotes the apoptosis of lung cancer cells by targeting SRC, PLoS One 9 (8) (2014) e105570.
[62] D. Zhao, et al., MicroRNA-203 inhibits the malignant progression of neuroblastoma by targeting Sam68, Mol. Med. Rep. 12 (4) (2015) 5554–5560.
[63] D. Pal, et al., Regulation of Cell Proliferation and Migration by miR-203 via GAS41/miR-10b Axis in Human Glioblastoma Cells, PLoS One 11 (7) (2016) e0159092.
[64] Z. Liu, L. Dong, Q. Dong, MicroRNA-203 inhibits proliferation and induces apoptosis of neuroblastoma SH-SY5Y cell via upregulation of TGF-B1/BIM signal, Int. J. Clin. Exp. Pathol. 10 (1) (2017) 341–349.
[65] M. Xu, et al., miR-203 inhibition of renal cancer cell proliferation, migration and invasion by targeting of FGF2, Diagn. Pathol. 10 (2015) 24.
[66] F. Zhang, et al., MiR-203 suppresses tumor growth and invasion and down-regulates MiR-21 expression through repressing Ran in esophageal cancer, Cancer Lett. 342 (1) (2014) 121–129.